A bispecific, crosslinking lectibody activates cytotoxic T cells and induces cancer cell death

Francesca Rosato
Albert-Ludwigs-Universitat Freiburg
Rajeev Pasupuleti
ACIB GmbH: Austrian Centre of Industrial Biotechnology
Jana Tomisch
Albert-Ludwigs-Universitat Freiburg
Ana Valeria Meléndez
Albert-Ludwigs-Universitat Freiburg
Dajana Kolanovic
ACIB GmbH: Austrian Centre of Industrial Biotechnology
Olga N. Makshakova
Albert-Ludwigs-Universitat Freiburg
Birgit Wiltschi
ACIB GmbH: Austrian Centre of Industrial Biotechnology
Winfried Römer (winfried.roemer@bioss.uni-freiburg.de)
Albert-Ludwigs-University Freiburg https://orcid.org/0000-0002-2847-246X

Research Article

Keywords: Lectins, Tumor-associated carbohydrate antigens, Bispecific targeting, Globotriaosylceramide, Click chemistry, Cancer immunotherapy, T cells, Shiga toxin

Posted Date: September 21st, 2022

DOI: https://doi.org/10.21203/rs.3.rs-2056554/v1

Abstract

Background

Aberrant glycosylation patterns play a crucial role in the development of cancer cells as they promote tumor growth and aggressiveness. Lectins recognize carbohydrate antigens attached to proteins and lipids on cell surfaces and represent potential tools for application in cancer diagnostics and therapy. Among the emerging therapeutic strategies, immunotherapy has become a promising treatment modality for various hematological and solid malignancies. Here we present an approach to redirect the immune system into fighting cancer by means of a “lectibody”, a bispecific construct that is composed of a lectin linked to an antibody fragment. This lectibody is inspired by bispecific T cell engager (BiTEs) antibodies that recruit cytotoxic T lymphocytes while simultaneously binding to tumor-associated antigens (TAAs) on cancer cells. The tumor-related glycosphingolipid globotriaosylceramide (Gb3) represents the target of this proof-of-concept study. It is recognized with high selectivity by the B-subunit of the pathogen-derived Shiga toxin, presenting an opportunity for clinical development.

Methods

The lectibody was realized by conjugating an anti-CD3 single-chain antibody fragment to the B-subunit of Shiga toxin to target $Gb3^+$ cancer cells. The reactive non-canonical amino acid azidolysine (AzK) was inserted at predefined single positions in both proteins. The azido groups were functionalized by bioorthogonal conjugation with individual linkers that facilitated selective coupling *via* an alternative bioorthogonal click chemistry reaction. *In vitro* cell-based assays were conducted to evaluate the antitumoral activity of the lectibody. Cytotoxic T lymphocytes (CTLs) isolated from healthy donors and Burkitt´s lymphoma-derived cells were screened in flow cytometry and cytotoxicity assays for their activation and lysis, respectively.

Results

This proof-of-concept study demonstrates that the lectibody activates T cells for their cytotoxic signaling, redirecting CTLs´ cytotoxicity in a highly selective manner and resulting in nearly complete tumor cell lysis – up to 93% – of $Gb3^+$ tumor cells *in vitro*.

Conclusions

This research highlights the potential of lectins for targeting of certain tumors, with an opportunity for new cancer treatments. In a combinatorial strategy, lectin-based platforms of this type offer the possibility to target glycan epitopes on tumor cells and boost the efficacy of current therapies, providing an additional strategy for tumor eradication and improving patient outcomes.

Background

Cancer is a leading cause of death worldwide, and according to the World Health Organization (WHO) it accounted for nearly 10 million deaths in 2020 [1]. Genetic and epigenetic alterations are recognized as primary causes of cancer development, where changes at the protein level drive cancer progression and dissemination [2]. Moreover, in the past decade glycobiology has gained increased importance in cancer research given its role in understanding cancer mechanisms and shining a new light on potential targets for diagnostic application and therapeutic strategies [3, 4]. Alterations in post-translational modifications such as glycosylation are indeed a common hallmark of cancer cells [5]. Cancer-associated glycans either occur as increased or incomplete branched-structures, appear as neoantigens, or as overexpressed or completely absent glycans [6, 7]. When cells evolve progressively to a neoplastic state, aberrant glycosylation of glycoproteins, glycosphingolipids and proteoglycans plays a crucial role in progression and invasiveness. These tumor-associated carbohydrate antigens (TACAs) contribute to proliferative signaling, the evasion of growth suppressors, resistance to cell death, angiogenesis, and the onset of cancer metastasis, leading ultimately to malignant phenotypes [5, 8]. Therefore, glycans have major potential applications in improving early diagnosis and determination of prognosis, as well as in serving as specific therapeutic targets. Novel strategies have been developed that focus on glycosylation patterns encountered in several cancers, with a major impact on emerging therapies [9].

Several TACAs consist of altered glycosphingolipids (GSLs) [10]. Among them, the glycosphingolipid Gb3 (α-D-Gal(1→4)β-D-Gal(1→ 4)β-D-Glc(1→O-ceramide), also known as CD77 or P^k antigen, has been reported to be overexpressed in Burkitt's lymphoma [11, 12], breast [13, 14], ovarian [15], colorectal [16, 17], and pancreatic cancer [18, 19]. Gb3 is present in the extracellular leaflet of the plasma membrane [20] and is mainly located in lipid rafts, which are membrane domains enriched in sphingomyelin and cholesterol. The ceramide backbone of this GSL is linked to a neutral trisaccharide composed of galactose (Gal) and glucose (Glc) [21]. Its cell surface-exposed oligosaccharide chains have been described as attachment sites for pathogens [22–24]. This receptor is exploited by different bacterial lectins/toxins [25], including Shiga toxins (Stxs) [26], for surface binding [27, 28] and uptake [29], intracellular trafficking, and signaling events [30–32]. Stxs (also termed verotoxins) are produced by *Shigella dysenteriae* serotype 1 and enterohaemorragic *Escherichia coli* (EHEC) strains [33–36] and belong to the AB_5 family of bacterial toxins. Additionally, some *E. coli* strains produce a second type of Stx, named Stx2, that has the same receptor and mode of action as Stx1, but is immunologically distinct and shares only 56% identity at the amino acid sequence level [37]. Stxs consist of an enzymatically active A-subunit that possesses *N*-glycosidase activity and inhibits protein biosynthesis by modifying host ribosomal RNA (rRNA), and a non-toxic, low immunogenic homopentameric B-subunit [38, 39]. The B-pentamer binds to its preferential globotriaosylceramide with high specificity and in a multivalent fashion [40, 41], presenting up to 15 binding sites for the receptor [42]. Upon binding to Gb3, StxB induces the formation of StxB-Gb3 cluster domains and imposes negative curvature on the host membrane, ultimately leading to lipid reorganization and the formation of narrow tubular membrane invaginations in cells and model membranes [40, 41]. Due to Gb3 implication in human cancers, Stx has found numerous

applications as cytotoxic agents or carriers for cytotoxic drugs in cancer treatment [43]. In particular, Shiga toxin 1 B-subunit (Stx1B) has been coupled to several chemotherapeutic compounds for targeting tumors, with excellent outcomes in intracellular transport of such drugs and elimination of cancer cells [18, 44–47]. The efficacy of these approaches suggests that Stx1B could be considered a promising tool for the selective targeting of carcinomas and lymphomas in which Gb3 is a TACA [11–15, 17, 35, 46, 48].

The specificity of several lectins, like the abovementioned Stx1B, towards carbohydrate antigens promotes their applications in biological and therapeutic research. In recent years, lectins have been investigated for a variety of novel medical approaches, including cancer diagnosis, imaging, targeted drug delivery and cancer treatment [49, 50]. By recognizing and binding mono- or oligosaccharides attached to proteins and lipids, lectins can be used to highlight and target precise distinctions in glycan structure or composition in the evolution of diseases [51, 52]. In cancer, cell surface alterations in glycan synthesis and expression constitute promising targets for lectin-based diagnosis and therapy. In such circumstances, lectins represent an opportunity to complement therapies based on glycan-binding antibodies targeting TACAs on malignant cells, as the development of such antibodies has been promising, but challenging. Indeed, in the past few decades few molecules have been evaluated in preclinical models and have progressed to clinical trials [53–59]. Antibodies represent an attractive class of therapeutics in the fast-developing field of immunotherapy. Remarkably, a large portion of novel treatments that aim at boosting the patients´ immune system in fighting cancer are based on monoclonal antibodies (mAbs), antibody-drug conjugates (ADCs), and bispecific antibodies (bsAbs) [57, 60]. In the mentioned examples, the anti-tumor activity of antibodies has been increased by engineering strategies that improve specific tumor-associated antigen (TAA) engagement. Of particular interest is the creation of bispecific antibodies that possess dual affinities for simultaneous recognition of distinct antigens. A promising approach to stimulate T cell immunity with bsAbs is the development of bispecific T cell engager (BiTE) molecules that target the CD3 receptor on T cells and a TAA on cancer cells, at the same time. Since Blinatumomab (MT103), the first CD19/CD3 BiTE approved by the United States Food and Drug Administration (FDA) in December 2014 for clinical use in patients with relapsed and/or refractory (R/R) non-Hodgkin lymphoma and R/R B cell precursor acute lymphoblastic leukemia (B-precursor ALL), this antibody format has seen a rapid development for the treatment of several malignancies [61]. So far, next-generation BiTEs against CD19, EpCAM or EGFR have faced clinical trials [62]. In the design of such antibodies, a CD3-targeted antibody fragment and a tumor antigen-targeted antibody are genetically linked, rendering it possible to activate a T cell when it physically engages a tumor cell and redirects its cytotoxic activity to achieve tumor cell lysis. The concept of retargeting T cell cytotoxicity for cancer therapy goes back to the 1970s, as these cells possess optimal therapeutic features for cancer [63]. T cells are indeed prone to rapidly expand upon activation and can be usually found in high numbers. They elicit strong cytotoxic responses and are able to attack tumor cells. Remarkably low doses of BiTEs can induce anti-tumor activity, and their efficacy is not affected by mutations of downstream signaling pathways that lead, for example, to resistance to monoclonal antibody-based treatments. In fact, T cell-engaging BiTE antibodies do not rely on the inhibition of TAA-induced signaling but use the TAA as surface anchor for attachment of cytotoxic T cells. As such, they bypass mutations in the cancer cells‘

signaling components, such as hyper activation of PI3-kinase and loss of PTEN for example [64, 65]. In view of the aberrant expression of certain GSLs in cancer, over the past two decades few antibodies have been evaluated in preclinical studies or clinical investigation. Examples include the mAb hu14.18K322A, which specifically recognizes the ganglioside GD2, evaluated in a phase II trial in neuroblastoma patients[66] and the mAb BIW-8962 against the ganglioside GM2, highly expressed in lung cancer [67]. However, glycans are considered poor immunogens[68, 69] and the challenging generation of high affinity antibodies against TACAs poses a limit to immunotherapy for the treatment of certain malignancies. For this reason, novel therapeutic approaches which employ recognition components other than antibodies are of particular interest.

In the present study, we successfully generated a bispecific T cell engager that replaces the tumor-targeted antibody fragment with a lectin to recognize TACAs. The single chain variable fragment (scFv) OKT3 was chosen as an anti-CD3-binding module [70, 71]. On the other end, the pentameric non-toxic B-subunit of the pathogen-derived Stx1 was selected for the targeting of Gb3-expressing malignant cells. The two proteins were genetically engineered to incorporate the non-canonical amino acid (ncAA) N6-((2-azidoethoxy)carbonyl)-L-lysine (AzK) at predefined permissive positions in their protein sequence. We used strain-promoted azide-alkyne cycloaddition (SPAAC) to functionalize the azido groups with linkers carrying compatible bioorthogonal groups that facilitated the conjugation of scFv OKT3 and Stx1B by inverse electron demand Diels-Alder (IEDDA) reaction. The conjugated product Stx1B-scFv OKT3 was denominated “lectibody”, based on its bispecific composition of a lectin and an antibody scFv. *In vitro* cell-based assays revealed that the Stx1B-scFv OKT3 lectibody can simultaneously engage cytotoxic T lymphocytes (CTLs) and $Gb3^+$ Burkitt´s lymphoma-derived cells, redirecting T cell cytotoxicity in a highly selective manner and resulting in nearly complete tumor cell lysis.

Material And Methods

Antibodies and chemicals

The following antibodies from BioLegend (San Diego, CA, USA) were used: biotin-labeled anti-human CD3 (UCHT1) (Cat. No. 300404), Pacific Blue™-labeled anti-hCD8 (Cat. No. 344718), APC-conjugated anti-hCD69 (Cat. No. 310909), FITC-conjugated anti-hCD71 (Cat. No. 334103), APC-labeled anti-hCD25 (Cat. No. 985810), Alexa Fluor 647-labeled anti-6-His epitope tag (Cat. No. 362611), FITC-conjugated anti-6-His epitope tag (Cat. No. 362618).

The following were obtained from commercial sources: RPMI 1640, DMEM, PBS, HEPES, FBS and L-glutamine were purchased from Gibco (Thermo Fisher Scientific Inc., Rockford, IL, USA). DMSO, penicillin/streptomycin, ß-mercaptoethanol, isopropyl-ß-D-1-thiogalactopyranoside (IPTG), Luria Bertani (LB) agar and Luria Bertani broth were obtained from Carl Roth GmbH & Co. (KG, Germany). D-Luciferin Firefly was provided by Biosynth (Staad, Switzerland), and Pancoll was purchased from PAN Biotech (Bayern, Germany). DL-threo-1-phenyl-2-palmitoylamino-3-morpholino-1-propanol (PPMP) was obtained from Sigma-Aldrich Chemie GmbH (Germany). All restriction enzymes (FastDigest) were purchased from

Thermo Fisher Scientific (Waltham, MA, USA). The Wizard® SV Gel and PCR Clean-Up System and Wizard® *Plus* SV Minipreps DNA Purification kit were obtained from Promega (Madison, WI).

Construction of expression vectors

Plasmids encoding Stx1B and Stx1B K9AzK were based on our previously published pT7x3 vector [72] with slight modifications. The Stx1B insert was produced by splicing two DNA fragments with overlapping sequences produced in two PCR steps. First, the Stx1B coding sequence with a C-terminal 6x histidine-tag was PCR amplified with primers 2609 F (5'-CATATGACGCCTGATTGTGTAACTGG-3'; NdeI site underlined) and 2607 R (5'-GAAGATCTTTATTAGTGATGGTGATGGTGATGGCCAG-3'; BglII site underlined) using an in-house plasmid [73] as the template. Secondly, a 95 bp sequence immediately upstream of the gene of interest (GOI) coding region in the target vector pT7x3 [72] was amplified with primers 2610F (5'-ACCGCTCGAGTAATACGACTCACTATAGGG-3'; XhoI site underlined) and 2608R (5'-CCAGTTACACAATCAGGCGTCATATGTAATTCTCCTTCTTAAAG-3'; NdeI site underlined). The reverse primer 2608R includes an ACT to CAT exchange upstream of the initiation codon (ATG) of the GOI to introduce an *NdeI* recognition site (CATATG) in the target vector p-T7x3 and modify it to pSCS-T7x31 for faciliated cloning. The two PCR products were spliced by overlap extension PCR following a published procedure [74]. The splice product was resolved on a 0.8 % (w/v) agaose gel and purified using the Wizard® SV Gel and PCR Clean-Up System. The purified insert and the target vector pSCS-T7x3 were digested with *XhoI/BglII* and ligated. Chemically competent *Escherichia coli* Top10 F' cells (Thermo Fisher Scientific Inc., Rockford, IL, USA) were heat shock transformed with the ligation mixture, regenerated, and plated on LB agar plates employing standard procedures [75]. Plasmids from selected kanamycin-resistant clones were isolated using the Wizard® *Plus* SV Minipreps DNA Purification kit and were sequenced (Microsynth AG, Balgach, Switzerland) using the 2609 F and 2607 R primers. The expression vector pSCS-T7x31-Stx1B K9am-6xH was constructed by PCR amplification of the Stx1B K9am gene from pSCS-Stx1B K9am [73] using primers 2609 F and 2607 R. We replaced the Stx1B coding sequence in pSCS-T7x31-Stx1B-6x H with the Stx1B K9am PCR product by restriction cloning using NdeI/BglII. Chemically competent *E. coli* BL21(DE3) cells (Merck KGaA, Darmstadt, Germany) were transformed with the sequence verified pSCS-T7x31-Stx1B-6x H and pSCS-T7x31-Stx1B K9am-6x H plasmids and stored in 30% (v/v) glycerol at -80°C. The construction of plasmids encoding scFv OKT3 and scFv OKT3 E129AzK will be described elsewhere.

Protein expression

To prepare an overnight pre-culture, 10 mL LB medium containing 50 µg/ml kanamycin (LBkan) were inoculated from the corresponding glycerol stock and were grown overnight (ON) at 37°C with 120 rpm shaking. 10 ml of ON culture was inoculated into 1-liter LBkan. The cultures were incubated at 37°C, shaking at 150 rpm, until the cell density (D_{600}) reached 0.8 for Stx1B and 0.5 for scFv OKT3. Protein expression was induced with 0.3 mM IPTG at 20°C for 16–19 hours, shaking at 180 rpm. For azide-labeled variants, freshly prepared non-canonical amino acid H-L-Lys(EO-N3)-OH*HCl (L-azidolysine or AzK; Iris Biotech, Marktredwitz, Germany) in sterile doubly distilled H_2O (ddH_2O) was added to a final concentration of 5 mM at the time of IPTG induction. Cells were harvested at 8000 rpm (JA-10.500 rotor,

Beckman Coulter Life Sciences, Indianapolis) for 15 minutes, and cell pellets stored at -20°C. scFv OKT3 and scFv OKT3 E129AzK were purified immediately after harvesting without storing the pellets.

Protein purification

To purify Stx1B and Stx1B K9AzK, the harvested cell pellets were thawed at room temperature (RT) and resuspended in 60 ml of immobilized metal affinity chromatography (IMAC) binding buffer (20 mM Tris, 300 mM NaCl, 10 mM imidazole; pH 8). Cells were physically disrupted using sonication (Branson Sonifier 250, Emerson Electric, St. Louis, MO, USA) for 3 minutes on ice. The lysed cell suspension was centrifuged at 21000 rpm for 20 minutes. The clarified cell lysate in the supernatant was added onto a Zn^{2+} charged sepharose matrix (Chelating Sepharose® Fast Flow, Cytiva, Marlborough, MA, USA) and the flow-through was collected by gravity. The matrix was washed with 25 mL IMAC wash buffer (20 mM Tris, 300 mM NaCl, 25 mM imidazole; pH 8) to remove non-specifically bound proteins. Column-bound protein was eluted with IMAC elution buffer (20 mM Tris, 300 mM NaCl, 400 mM imidazole; pH 8) and collected in 1 ml fractions. The absorbance of the fractions was measured using a spectrophotometer (Thermo Scientific Inc., Rockford, IL, USA) at 280 nm. The fractions with the highest absorbance were pooled and the buffer was exchanged to phosphate-buffered saline (PBS, 137 mM NaCl, 2.7 mM KCl, 10 mM Na_2HPO_4, and 1.8 mM KH_2PO_4, pH 7.4) using PD-10 desalting columns (GE Healthcare, Boston, MA, USA) prior to lyophilization. At every step, protein gel samples (PGS) of 12 µl were mixed with 3 µl of 5 X reducing sample buffer (250 mM Tris, 20% (v/v) glycerol, 5% SDS, 500 mM dithiothreitol, 0.2% (w/v) bromophenol blue, 2.5% (v/v) ß-2mercapto ethanol) and heated at 95°C for 5–10 minutes before analysis by SDS-PAGE. The purification and analysis of scFv OKT3 and scFv OKT3 E129AzK will be described elsewhere.

Stx1B and scFv OKT3 labelling

The proteins with a final concentration Stx1B (5 µM), Stx1B K9AzK (5 µM), scFv OKT3 (2 µM) and scFv OKT3 E129AzK (2 µM) were separately mixed with a ten-times excess of dibenzocyclooctyne-sulfo-Cy3 (DBCO-Cy3, Jena Bioscience GmbH) in 10 µl volumes in PBS at 22°C and incubated with shaking at 600 rpm for 1 hour in the dark.5 XSDS reducing sample buffer was added directly to the sample to stop the SPAAC reaction. For cell-based assays, commercial Stx1B (Sigma-Aldrich Chemie GmbH, Germany) was dissolved at 1 mg/mL in PBS and stored at 4°C prior to its use. For fluorescence labelling, Cy5 mono-reactive NHS ester (GE Healthcare, Boston, MA, USA) was used. The fluorescent dye was dissolved at a final concentration of 10 mg/mL in water-free DMSO, aliquoted, and stored at − 20°C before usage according to the manufacturer´s protocol. For the labelling reaction, 100 µL of Stx1B (1 mg/mL) was supplemented with 10 µL of a 1 M $NaHCO_3$ (pH 9) solution so that the molar ratio between dye and lectin was 6:1. The labelling mixture was incubated at 25°C for 60 minutes under continuous stirring, and uncoupled dyes were removed using Zeba™ Spin desalting columns (7 kDa MWCO, 0.5 mL, Thermo Fischer Inc., Rockford, IL, USA). Cy5-labelled Stx1B was stored at 4°C with protection from light.

Conjugation of Stx1B and scFv OKT3

The lyophilized Stx1B K9AzK and scFv OKT3 E129AzK were resuspended in sterile ddH_2O, and the concentrations were measured spectrophotometerically. The linkers methyltetrazine (Tz)-DBCO and *trans*-cyclooctene (TCO)-PEG4-DBCO from Broadpharm (San Diego, CA) were dissolved in DMSO to a concentration of 100 mM and stored as 10 µl aliquots at -20°C in the dark until use. SPAAC was performed at RT for 2 hours in 100 µL volumes of PBS (pH 7.4) containing 60 µM Stx1B K9AzK and 600 µM methyltetrazine-DBCO or 20 µM scFv OKT3 E129AzK and 200 µM TCO-PEG4-DBCO. The DMSO concentration was maintained between 8–10% (v/v) in the reaction mixtures. To stop the reaction and to remove the unreacted linkers, the reaction mixture was buffer exchanged with PBS (pH 7.4) using 0.5 ml Zeba Spin desalting columns. IEDDA was performed according to [76] by mixing a three-times excess of Stx1B K9Tz to scFv OKT3 E129-PEG4-TCO at RT for 1.5 hour. The IEDDA reaction mixture was separated by gel filtration chromatography (see sections below). For SDS-PAGE analysis, an aliquot of the sample was mixed with 5 X SDS reducing sample buffer at a ratio of 1:5.

Electrophoresis

SDS-PAGE: 4–12% NuPAGE bis-tris mini protein precast polyacrylamide gels (Invitrogen) were run for 40 minutes at 200 V with NuPAGE MES-SDS running buffer (Thermo Fisher Scientific). The gels were stained with InstantBlue® Coomassie Protein Stain (Abcam plc., UK). Gels with fluorophore-labelled samples were washed three times for 15 minutes each and observed for fluorescence at 635 nm (G:Box F3 gel doc system, SYNGENE, UK) before staining with InstantBlue® Coomassie Protein stain. Native-PAGE: The SERVA*Gel*™ N Native Starter Kit (Serva Electrophoresis GmbH, Heidelberg) was used to run clear native electrophoresis with the native cathode and anode buffers. Two micrograms of Stx1B K9AzK were mixed with 2 X clear native sample buffer (100 mM NaCl, 100 mM imidazole, 4 mM 6-aminocaproic acid, 2 mM EDTA, 0.02% (w/v) Ponceau S, 20% (v/v) glycerol) and resolved on a 3–12% vertical native gel at 50 V for 10 minutes, and 200 V for 90 minutes. The gels were developed by silver staining as described in [77].

Gel filtration chromatography

Superdex 200 Increase 10/300 GL column (Cytiva) was used for a small-scale preparative purification and characterization of the Stx1B-scFv OKT3 conjugate. The column was connected to an ÄKTA pure chromatography system (GE Healthcare) and calibrated with molecular weight standards aprotinin (6500 Da), ovalbumin (43000 Da), conalbumin (75000 Da), aldolase (158000 Da) and ferritin (440000 Da) from GE Healthcare. Theoretical molecular weights for scFv OKT3 and STx1B-scFv OKT3 were calculated using Protparam Expasy [78].

Mass spectrometry

Proteins were desalted using Amicon centrifugal filters before analysis. A volume of 5 µl protein with a concentration ranging between 0.1–0.3 mg/ml was injected into a LC-ESI-MS system (LC: Agilent 1290 Infinity II UPLC). A gradient from 15 to 80% acetonitrile in 0.1% (v/v) formic acid (using a Waters BioResolve column (2.1 x 5 mm)) at a flow rate of 400 µL/min was applied (9-minute gradient time). A Q-TOF instrument (Agilent Series 6560 LC-IMS-QTOFMS) equipped with the Jetstream ESI source in positive ion, MS mode (range: 100–3200 Da) was used for detection. ESI calibration mixture (Agilent) was used to

calibrate the instrument. MassHunter BioConfirm B.08.00 (Agilent) was used for data processing and the spectrum was deconvoluted by MaxEnt.

Isothermal titration calorimetry

MicroCal PEAQ-ITC (Malvern Panalytical ltd, Malvern, UK) microcalorimeter was used to perform ITC experiments. Lyophilized Stx1B and Stx1B K9AzK were dissolved in sterile ddH_2O. Buffer was exchanged to PBS (pH 7.4) using PD-10 desalting columns. Globotriose (Gb3) (ELICITYL, Crolles, Frances) was resuspended in the same buffer. Gb3 (50 mM) was titrated into the sample cell with 190 µM Stx1B or Stx1B K9AzK in a total of fourteen 2.8 µl injections, each spaced at 300 seconds. Data were analysed using a one-site binding model in Microcal origin (OriginLab, Northampton, MA, USA).

Structural modelling

The structural model of the lectibody was constructed on the base of StxB 3D structure (PDB code 1BOS) and structural information about OKT3 Fab from *Mus musculus* (PDB code 1SY6). The fragments of heavy and light chains of OKT3 Fab that shared high percentage of identity with scFv OKT3 were used as a template for the homology modelling of scFv OKT3. The mutual orientation of domains in the resultant protein was kept the same as in the template. The homology modelling was performed using the Modeller program v9.15 [79]. The StxB and scFv OKT3 were linked *via* the DBCO-methyltetrazine-DBCO linker. The assembled structure was energy minimized in OPLS2005 force field implemented in Maestro Schrodinger [80] using the Polak-Ribier Conjugate Gradient method [81] with a gradient convergence threshold of 0.05 $kJ \cdot mol^{-1} \cdot Å^{-1}$.

Cell lines

Human Jurkat T cells (American Type Culture Collection, TIB-152, Thermo Fisher Scientific Inc., Rockford, IL, USA), HEK293T cells, Burkitt´s lymphoma Ramos and Namalwa cell lines were used in this study (Ramos cells were kindly provided by Prof. Dr. Michael Reth, Institut für Biologie III, Albert-Ludwigs Universität Freiburg, Germany; NAMALWA.CSN/70, ACC 70, DSMZ - German Collection of Microorganisms and Cell Cultures GmbH). Ramos and Namalwa cells were transduced with lentiviruses harboring the plasmid pHRSIN-CS-Luc-IRES-emGFP (this plasmid and HEK293T cells were kindly provided by PD Dr. Susana Minguet, Institut für Biologie III, Albert-Ludwigs Universität Freiburg, Germany). Jurkat T cells were maintained in Roswell Park Memorial Institute (RPMI) 1640 medium supplemented with 10% (v/v) heat-inactivated fetal bovine serum (FBS), 2 mM L-glutamine, 2.5 µg/mL penicillin/streptomycin, 0.1% (v/v) of a phosphate-buffered saline (PBS) solution containing ß-mercaptoethanol, 1% (v/v) HEPES in a humidified incubator with 5% CO_2 at 37°C. Ramos and Namalwa cells were cultivated in RPMI 1640 medium containing 10% (v/v) FBS, 2 mM L-glutamine and 5 µg/mL penicillin/streptomycin. HEK293T cells were grown in a humidified incubator with 7.5% CO_2 at 37°C in Dulbecco's Modified Eagle Medium (DMEM) medium complemented with 10% (v/v) FBS, 2.5 µg/mL penicillin/streptomycin, 0.1% (v/v) of PBS solution containing ß-mercaptoethanol, 1% (v/v) sodium pyruvate. If not stated differently, all experiments were performed in the described complete media.

Lentiviral transduction

A total of 10^7 HEK293T cells were plated and incubated overnight. After medium exchange, the HEK293T cells were transfected with the packaging plasmid pMD2.G, the gag/pol pCMVR8.74 and the plasmid pHRSIN-CS-Luc-IRES-emGFP (kindly provided by PD Dr. Susana Minguet, Institut für Biologie III, Albert-Ludwigs Universität Freiburg, Germany) using Polyethylenimine (PEI) (Polysciences Inc., Warrington, PA, USA) transfection. The medium containing lentiviral particles was collected at 24 and 48 hours post-transfection and concentrated by a 10% sucrose gradient. After 4 hours of centrifugation at 10000 rpm (Rotor FA-45-6-30, Eppendorf SE, Hamburg, Germany) and 6°C, the supernatant was discarded, and the virus pellet was resuspended in PBS to be stored at -80°C. Concentrated lentiviruses were used to transduce Ramos and Namalwa cells from Burkitt´s lymphoma by spin infection [82] (multiplicity of infection of 10). Afterwards, B cells were cultured with the lentiviruses in RPMI 1640 medium, at 37°C for 48 hours.

Primary human T cells isolation

Peripheral blood mononuclear cells (PBMCs) were isolated from leukoreduction system chambers using density centrifugation (Pancoll human), according to the BioSharing protocol [83]. PBMCs were adjusted to 10^6 cells/mL and cultured in RPMI 1640 supplemented with 10% (v/v) fetal bovine serum (FBS), 2 mM L-glutamine, 2.5 µg/mL penicillin/streptomycin, 0.5% (v/v) of a PBS solution containing ß-mercaptoethanol, 1% (v/v) HEPES in a humidified incubator with 5 % O_2 at 37°C, or frozen in cryovials (20×10^6 cells per vial, in 0.5 mL FBS solution containing 10% (v/v) sterile DMSO) for long-term preservation.

Depletion of glucosylceramide-based glycosphingolipids by PPMP treatment

To deplete Ramos cells of globotriaosylceramide, 2×10^5 cells were seeded in 6-well plates and cultured for 72 hours in the presence of 2 µM DL-threo-1-phenyl-2-palmitoylamino-3-morpholino-1-propanol (PPMP), an inhibitor of the synthesis of glucosylceramide-based GSLs [84]. Depletion of globotriaosylceramide from the plasma membrane of treated cells was assessed by flow cytometry analysis by using 2.6 nM Stx1B-Cy5 in binding assays.

Flow cytometry

For flow cytometry sample preparation, cells were counted and transferred to a U-bottom 96 well plate (Sarstedt AG & Co. KG, Numbrecht, Germany). For binding assays, Ramos, Namalwa and Jurkat T cells were resuspended to a concentration of 1×10^5 cells/well, while PBMCs were used at a final concentration of 2×10^5 cells/well. To quantify binding of wild type Stx1B-Cy5, mutant Stx1B K9AzK and lectibody (Stx1B-scFv OKT3) to cell surface receptors, cells were incubated with proteins for 30 minutes on ice, compared to PBS-treated cells as the negative control. Subsequently, cells were centrifuged at 1600 x g for 3 minutes on ice and washed twice with FACS buffer (PBS supplemented with 3% FBS v/v). Cells were stained with fluorescently labelled anti-6-His epitope tag Alexa Fluor 647 antibody diluted in

FACS buffer, for 20 minutes on ice and protected from light. For the characterization of CD3 antigens at the membrane, cells were incubated with anti-human CD3 FITC antibody (OKT3 clone), for 20 minutes on ice. At the end of incubation, cells were centrifuged and washed twice as described above. After the last washing step, the cells were resuspended with FACS buffer and transferred to FACS tubes (Kisker Biotech GmbH Co. KG, Steinfurt, Germany). The fluorescence intensity of treated cells was monitored immediately at FACS Gallios (Beckman Coulter Inc., USA) and further analyzed using FlowJo V.10.5.3 (FlowJo LLC, BD).

Cytotoxicity assay

For the Bioluminescence-based cytotoxicity assay, luciferase-expressing Ramos and Namalwa tumor cells were counted and plated at a concentration of 1.5×10^4 cells in 96-well white flat bottom plates in duplicates. Then, 75 µg/mL of D-firefly luciferin potassium salt was diluted in complete medium and added to the tumor cells. Bioluminescence (BLI) was measured in the luminometer (Tecan infinity M200 Pro) to establish the BLI baseline. Subsequently, PBMCs isolated from healthy donor cells were added at 5:1 effector-to-target (E:T) ratio, and BLI was recorded at several times (4, 8, 24 or 48 hours) after incubation at 37°C. The Stx1B-scFv OKT3 lectibody was added in two different concentrations (7 nM and 35.6 nM) to the samples, as indicated. BLI was measured as relative light units (RLUs). RLU signals from tumor cells cultured with PBMCs cells in absence of lectibody determine spontaneous cell death. RLU signals from cells treated with 2% Triton X-100 indicate maximal cell death. Percent of specific killing was calculated with the following formula: percentage specific killing = 100 × (average spontaneous death RLU − test RLU) / (average spontaneous death RLU − average maximal death RLU).

CD69, CD71 and CD25 upregulation assay

PBMCs were co-cultured with target cells in a 5:1 E:T ratio in presence or absence of Stx1B-scFv OKT3 lectibody. 3×10^5 PBMCs were counted per well and incubated with 6×10^4 Ramos or Namalwa, as indicated. Cells were treated with 35.6 nM lectibody or left untreated in PBS-containing medium. The plate was incubated at 37°C and 5% CO_2 for 24 or 48 hours. After incubation, cells were centrifuged at 1600 x g for 3 minutes on ice and washed twice with FACS buffer (PBS supplemented with 3% FBS v/v). Cells were stained with fluorescently labelled APC-conjugated anti-hCD69, FITC-conjugated anti-hCD71, APC-labeled anti-hCD25 antibodies diluted in FACS buffer, for 20 minutes on ice and protected from light. At the end of incubation, cells were centrifuged and washed twice as described above. After the last washing step, the cells were resuspended in FACS buffer and transferred to FACS tubes (Kisker Biotech GmbH Co. KG, Steinfurt, Germany). The fluorescence intensity of treated cells was monitored immediately at FACS Gallios (Beckman Coulter Inc.) and further analyzed using FlowJo V.10.5.3 (FlowJo LLC, BD).

Statistical analysis

All data in graphs are presented as mean ± standard deviation (SD) and were calculated from the results of independent experiments. Statistical testing was performed with GraphPad Prism software and Microsoft Excel using data of ≥ 3 biological replicates. Statistical differences in independent, identical samples were determined with a two-tailed, unpaired t-test. Tests with a p-value ≤ 0.05 are considered

statistically significant and marked with an asterisk (*). *p*-values ≤ 0.01 are shown as two asterisks (**), and ≤ 0.001 are summarized with three asterisks (***).

Results

Prediction of the Stx1B-scFv OKT3 structure

For the rational design of the lectibody construction, the 3D structures of Stx1B from *Shigella dysenteriae* and the murine hybridoma scFv OKT3 that recognizes an epitope on the human CD3ε subunit of the T cell receptor (TCR) complex were analyzed. The AzK residue was incorporated in protein sequences according to the following conditions: 1) the ncAA should be located at the surface of protein; 2) the residue should be inserted at a distance from the receptor (Gb3 or CD3) binding site, to avoid interference with the binding; 3) the residues in five monomers should be located at a distance from each other to facilitate their derivatization. In the Stx1B sequence, the K9 amino acid, oriented such that it opposes the glycolipid binding pockets facing the membrane (Fig. 1a), suits this purpose perfectly. The residue E129 in the linker connecting the two domains in scFv OKT3 was chosen to site-specifically incorporate AzK (Fig. 1b). The attached linker does not take part in the CD3 recognition, and the amino acid substitution and modification in this region should not destabilize the protein structure nor the receptor binding. Further analysis showed that, at the chosen length of the linkers, the scFv domains do not sterically interfere with each other and all five sites at Stx1B can be theoretically occupied by scFv OKT3 antibody fragments (Fig. 1c, d).

Construction of the Stx1B-scFv OKT3 conjugate

We chose position K9 of Stx1B for incorporating AzK and subsequent conjugation of scFv OKT3 since this position is surface exposed and distant from the glycan recognition site [73, 85]. The scFv OKT3 sequence included the double mutations E6Q and C105S for soluble expression [86] and a PelB signal sequence for delivery to the periplasm. We employed the pyrrolysyl-tRNA synthetase from *Methanosarcina mazei* with its cognate amber suppressor $tRNA_{CUA}$ (orthogonal *Mm*PylRS/*Mm*$tRNA_{CUA}$ pair [87]) for the site-specific incorporation of AzK [72] in response to in-frame amber codons at positions K9 and E129 of Stx1B and scFv OKT3, respectively. The corresponding wild-type genes were expressed as benchmark controls. Stx1B and Stx1B K9AzK were expressed and purified from the cytosolic soluble protein fraction as described previously [73] while scFv OKT3 and scFv OKT3 E129AzK were produced in the soluble periplasmic fraction. The amber mutants were only expressed when AzK was supplemented in the culture medium (Fig. S1a), while no expression occurred in its absence (Fig. S1b), which confirmed the fidelity of the orthogonal *Mm*PylRS/*Mm*$tRNA_{CUA}$ pair. The titres of the purified proteins per litre of culture medium were 3 mg for Stx1B, 2.8 mg for Stx1B K9AzK (93 % of the wild-type, 2 mg for scFv OKT3 and 1.4 mg for scFv OKT3 E129AzK (70 % of the wild type.

We assessed the incorporation of AzK into Stx1B K9AzK and scFv OKT3 E129AzK by labelling the purified proteins with the DBCO-Cy3 fluorophore *via* SPAAC. The unmodified wild-type proteins were used

as a negative control. The proteins containing AzK showed fluorescence at 635 nm indicating Cy3 labelling (Fig. 2), whereas no fluorescence was observed with Stx1B and scFv OKT3 which lacked AzK. This observation confirmed the successful incorporation of AzK into Stx1B and scFv OKT3. Mass analysis of the intact proteins further confirmed the incorporation of AzK in Stx1B K9AzK and scFv OKT3 E129AzK (Fig. S2, Table S1). Stx1B K9AzK monomers in solution oligomerized into a pentamer (Fig. S1c), which is a prerequisite for the biological function of Stx1B. Finally, ITC analysis confirmed that Stx1B and Stx1B K9AzK bound Gb3 with millimolar K_D values (Fig. S3) comparable to previous studies [88].

The Stx1B-scFv OKT3 lectibody was assembled *via* two click reactions, SPAAC and IEDDA. The SPAAC reaction is a cycloaddition of a cyclic alkyne (e.g. dibenzocyclooctyne DBCO) and an organic azide (e.g. AzK) leading to a stable triazole product [89]. Whereas IEDDA involves the reaction between electron-poor dienes (e.g. tetrazines) and electron-rich dienophiles (e.g. *trans*-cyclooctenes) to form dihydropyridazines [90]. As illustrated in the scheme in Fig. 3a, we first exploited the azido groups on Stx1B K9AzK and scFv OKT3 E129AzK to install a DBCO-methyltetrazine- and a DBCO-PEG4-*trans*-cyclooctene linker, respectively, by SPAAC. In a second step, the tetrazine-functionalized Stx1B was conjugated with scFv OKT3 carrying the *trans*-cyclooctene-moiety by the IEDDA reaction to form the Stx1B-scFv OKT3 conjugate. The SDS-PAGE analysis of the IEDDA reaction mixture (lane 4 of the SDS gel shown in Fig. 3b) revealed the monomeric Stx1B-scFv OKT3 conjugate at an apparent molecular weight of 50 kDa (MW_{calc} 39 kDa) as well as unreacted Stx1B K9AzK at ~ 12 kDa (MW_{calc} 9 kDa) and scFv OKT3 E129AzK at 37 kDa. (MW_{calc} 30 kDa). The band below 70 kDa most probably corresponds to an impurity in the scFv OKT3 E129AzK preparation. Mass analysis of the in-gel tryptic digest of the band at 50 kDa excised from the SDS gel (lane 4, Fig. 3b) was confirmed as Stx1B-scFv OKT3 conjugate (Table S2). The Stx1B-scFv OKT3 conjugate was purified from the reaction mixture by size exclusion chromatography (SEC) and re-run on an SDS gel, which showed the monomeric Stx1B-scFv OKT3 conjugate and unreacted Stx1B K9AzK but no unreacted scFv OKT3 E129AzK (Fig. 3b, lane 3). This finding indicates that not all five subunits in a Stx1B pentamer were conjugated with scFv OKT3. We deduced from the SEC analysis (Fig. S4) that three scFv OKT3 molecules were conjugated to one Stx1B pentamer (Table S3).

Binding specificity and affinity of Stx1B-scFv OKT3 lectibody to cell surface expressed antigens

The ability of the generated lectibody to recognize the Gb3 and CD3 antigens as cell surface receptors was studied by flow cytometry. The neutral glycosphingolipid Gb3 is commonly indicated as the B-cell differentiation antigen CD77 or BLA (Burkitt's lymphoma-associated antigen). It is expressed on a subset of germinal center B cells [91] and present in high amounts on Burkitt's lymphoma (BL) cells [92]. Previous studies by Taga et al. reported that the ligation of Gb3 by specific mAbs induces apoptosis in Burkitt's lymphoma [93], and the nature of the apoptotic signals mediated by Gb3 was later on examined by Tétaud et al. [94]. This prompted us to investigate the anti-tumor activity of the Stx1B-scFv OKT3 lectibody in Burkitt's lymphoma-derived cell lines. We included the Gb3-expressing ($Gb3^+$) B cell line Ramos in our study, as well as the Gb3-negative (Gb3) cell line Namalwa as a negative control. The

expression of the GSL Gb3, as well as the absence of the CD3 complex on each cell line, was assessed by flow cytometry using fluorescently labelled Stx1B-Cy5 and anti-human CD3 FITC antibody (Figs. S5a). Similarly, the recognition of CD3 antigens by the Stx1B-scFv OKT3 lectibody was evaluated on cultured human Jurkat T cells and on peripheral blood mononuclear cells (PBMCs) isolated from healthy anonymous donors. The presence of CD3 receptors at the surface of the tested cells was first monitored by flow cytometry using an anti-human CD3 FITC antibody, and the absence of Gb3 receptors by using Stx1B-Cy5, to exclude unwanted cross-binding (Fig. S5b). The specificity of the Stx1B K9AzK mutant towards Gb3 antigens on Ramos and Namalwa cells was then compared to that of Stx1B wild type in flow cytometry analysis (Figs. S6a, b). In a similar manner, the recognition of CD3 antigens by scFv OKT3 wild type and the scFv OKT3 E129AzK variant was detected by binding to Jurkat T cells surface (unpublished observation by the authors, manuscript in preparation). Cell-binding assays in Figs. S5 and S6 confirmed the presence of the intented target receptors on the tested cell lines and the absence of off-target interactions on such cells from Stx1B K9AzK scFv OKT3 E129AzK mutants.

To examine the binding of conjugated Stx1B-scFv OKT3 to tumor and effector cells, the lectibody was incubated with Ramos, Namalwa, Jurkat cells and PBMCs for 30 minutes on ice (Fig. 4). A panel of different lectibody concentrations was used, spanning from 350 pM to 35.6 nM. At the end of incubation, cells were washed twice to remove the unbound protein and subsequently stained with fluorescently labeled anti-6-His epitope tag AF647 antibody to detect the presence of the Stx1B-scFv OKT3 lectibody at the cell surface. As depicted in Fig. 4a, Ramos cells, which are $Gb3^+$, were positive at all the tested concentrations, showing a dose-dependent trend in lectibody binding in flow cytometry analysis. We did not record changes in fluorescence intensity for the Gb3 Namalwa cells, indicating the absence of unspecific recognition and binding by the Stx1B-scFv OKT3 lectibody (Fig. 4b). On the other hand, Jurkat T cells and PBMCs (Figs. 4c and d, respectively), were positive at all tested concentrations as well, and showed binding of the lectibody to CD3 receptors at the plasma membrane for higher concentrations of Stx1B-scFv OKT3 compared to Ramos cells, and in a dose-dependent manner.

To further demonstrate the specificity of the Stx1B-scFv OKT3 lectibody in targeting the GSL Gb3, $Gb3^+$ Ramos cells were treated with the endogenous glucosylceramide synthase (GCS) inhibitor DL-threo-1-phenyl-2-palmitoylamino-3-morpholino-1-propanol (PPMP). To inhibit the synthesis of glucosylceramide-based GSLs and thus deplete Gb3 abundance at the plasma membrane, Ramos cells were incubated with 2 μM PPMP for 72 hours before flow cytometry analysis. Subsequently, cells were treated with 3.5 nM of Stx1B-scFv OKT3 for 30 minutes on ice, and samples were analyzed for the binding of the lectibody to target cells after staining with anti-6-His epitope tag AF647 antibody as indicated above (Fig. 5a).

Control Ramos cells, in which Gb3 synthesis was preserved, are shown in the left histogram of Fig. 5a, while PPMP-treated Ramos cells are reported on the right side. Histograms of fluorescence intensities revealed a significant reduction in binding of the lectibody to the plasma membrane from 87.8–0.51% compared to untreated cells for the tested concentration (3.5 nM). These results corroborate those obtained from Fig. 4b, where the absence of Gb3 on Namalwa cells determined the absence of binding of the Stx1B-scFv OKT3 construct.

In a similar manner, PBMCs were treated with an excess of anti-human CD3 antibody, competing with the lectibody for the CD3 receptors at the cell surface. Figure 5b displays flow cytometry analysis of control PBMCs (left plot) and anti CD3-treated PBMCs (right plot) after incubation with the Stx1B-scFv OKT3 lectibody. Upon saturation of CD3 receptors with 0.5 µM of anti-human CD3 antibody, the fluorescence signal for the binding of the lectibody to treated cells decreased drastically, from 49.8% in the untreated control to 5.9% for anti CD3-treated PBMCs, as shown by the shift of the histogram towards lower values of fluorescence intensity. Taken together, these results support the functional affinity and specificity of the clicked scFv OKT3 and Stx1B domains of the lectibody for target and effector cells.

Redirected killing of Gb3-positive cancer cells by the Stx1B-scFv OKT3 lectibody

Next, we tested the efficacy of the generated lectibody in inducing T cell-mediated killing of $Gb3^+$ tumor cells. The Stx1B-scFv OKT3 lectibody could redirect unstimulated peripheral T cells to lyse $Gb3^+$ Ramos cancer cells in a concentration-dependent fashion. PBMCs and target cells were co-cultured in presence of the lectibody for 48 hours, and elimination of target cells was recorded as bioluminescence (BLI) at several times (4, 8, 24 and 48 hours). Efficacy of tumor cell lysis was investigated in presence of 7 nM or 35.6 nM lectibody, with the effector to target (E:T) ratio adjusted to 5:1. Control samples included PBMCs and target cells co-incubated in absence of lectibody, counted as spontaneous cell death. Figure 6 presents graphs of *in vitro* killing activity, expressed as percentage of specific killing induced by Stx1B-scFv OKT3. Strikingly, $Gb3^+$ Ramos cells were efficiently eliminated by the treatment at low nanomolar concentrations. As reported in Fig. 6a, lower concentrations of Stx1B-scFv OKT3 (7 nM) induced around 40% of tumor cell lysis at 24 hours, followed by an increase in cell death for Ramos to about 70% at 48 hours. Remarkably, the higher lectibody concentration of 35.6 nM mediated tumor cell killing at earlier time points (around 40% at 8 hours post-treatment) and affected 72% of tumor cell death after 24 hours. At 48 hours post-treatment with the lectibody we recorded 93% of tumor cell elimination. Furthermore, flow cytometry analysis of Ramos cells and PBMCs revealed that the Stx1B-scFv OKT3 lectibody can be detected at the plasma membrane of treated cells after 24 and 48 hours incubation, indicating a stable binding of the lectibody to surface antigens (Figs. S7a, b). On the other hand, Gb3 Namalwa cells were resistant to being targeted by the treatment for both tested concentrations (Fig. 6b). Similarly, cytotoxicity towards PPMP-treated Ramos cells (Fig. 6c) was not recorded, confirming poor or no activity of the Stx1B-scFv OKT3 in absence of the target receptor, the GSL Gb3.

Induction of T cell activation by Stx1B-scFv OKT3

T cell activation is a tightly regulated cascade of events that lead to the induction of cytokines and expression of activation molecules, resulting in divergent immune responses [95]. Analysis of qualitative and quantitative T cell activation following immunological treatments provides valuable information about the type of immune responses mediated by such therapies. The existence of a tumor-specific CTL response in this study is strengthened by identification of T cell activation markers on the surface of $CD8^+$ T lymphocytes. Upon T cell stimulation, the upregulation of several molecules is different for each

stage of the activation process. Such activation markers can be detected on the cell surface of T cells using flow cytometry. Hence, we investigated the ability of Stx1B-scFv OKT3 lectibody to trigger effective signaling downstream of CD3 stimulation and induce the surface expression of CD69 (very early), CD71 (middle) and CD25 (late) activation markers on $CD8^+$ cytotoxic T cells.

The earliest activation marker is CD69, an inducible cell surface glycoprotein expressed following activation via the TCR and its associated CD3 complex. CD69 is reported to play a role in the proliferation and survival of activated T lymphocytes [96, 97]. It is expressed at low basal levels in resting lymphocytes, while its transcription increases upon activation of T cells in a time-dependent manner between 3 and 12 hours, and its expression remains elevated until 24 hours, declining thereafter [98]. Accordingly, we detected the presence of elevated CD69 expression at the surface of $CD8^+$ T cells following treatment with the lectibody. Unstimulated PBMCs from healthy donors were co-cultured with target cells in the presence of 35.6 nM lectibody for 24 or 48 hours, and Mean Fluorescence Intensity (MFI) was calculated following flow cytometry analysis. At 24 hours, CD69 results increased in the co-presence of $Gb3^+$ Ramos cells and Stx1B-scFv OKT3, while its expression remained at basal levels when PBMCs were incubated solely with Stx1B-scFv OKT3, or increased only slightly when in the presence of Gb3 Namalwa cells and Stx1B-scFv OKT3 (Fig. 7a).

CD71, also named Transferrin Receptor (TfR), is a cell surface iron transport receptor that is upregulated in proliferating cells by 24–48 hours following T cell activation. Thus, CD71 can be considered a mid-activation marker. This receptor has been shown to physically associate with the TCRζ chain and ZAP70 tyrosine kinase, suggesting that it could promote signal amplification upon antigen binding to the TCR [99]. Moreover, CD71 is an essential factor for proliferating T cells [100]. Our results in Figs. 7b and c indicate an increase in the surface expression of this marker, similarly to our observation with CD69. $CD8^+$ T cells present the highest CD71 expression at both 24 and 48 hours in the presence of Gb3-expressing tumor cells and lectibody.

CD25 is the α-chain of the trimeric interleukin-2 (IL-2) receptor. It is considered the most pronounced cellular activation marker. It is constitutively expressed on the surface of several subsets of T lymphocytes, including regulatory and resting memory T cells. Following stimulation of the TCR/CD3 complex, CD25 is upregulated within 24 hours and remains elevated for a few days [98, 101]. It is involved in T cell responsiveness to IL-2, resulting in lymphocyte activation and further IL-2 production, an event that determines survival, expansion and function of T lymphocytes. We determined the expression of CD25 on CTLs at 48 hours post-treatment with the lectibody. As depicted in Fig. 7d, surface expression of CD25 in $CD8^+$ T cells followed a similar trend to the previously described CD69 and CD71 activation markers. The induction of CD25 expression on T cells was relevant when they were stimulated with Stx1B-scFv OKT3, but only in the presence of $Gb3^+$ tumor cells.
Collectively, our data show that the expression of CD69, CD71 and CD25 activation markers follows a precise and consistent time-course, where changes in CD71 expression proved to be the most prominent.

Moreover, the recorded activation of CTLs is specifically driven by the treatment with the Stx1B-scFv OKT3, only for the $Gb3^+$ target cells.

Discussion

Selective targeting of cancer cells is a crucial requirement for the improvement of anti-tumor therapies to avoid toxicity in non-neoplastic cells [102]. It is becoming evident that certain altered glycans aiding tumor onset and progression can be used as selective targets for improved diagnostics and therapeutic strategies. Here, we present a novel bispecific lectibody that targets the glycosphingolipid Gb3 on Burkitt´s lymphoma-derived cell lines and engages T cells for a specific and powerful anti-tumor response. The format of a bispecific lectibody is inspired by the therapeutic class of BiTEs, which have proven efficient in redirecting immune cells, primarily T cells, towards target cells, thereby inducing anti-tumor activity. For example, the CD19 × CD3 canonical BiTE blinatumomab has achieved impressive efficacy in treating B cell malignancies [103]. Therefore, our study aimed to show that a bispecific lectibody with the lectin Stx1B as tumor-targeting domain and scFv OKT3 as a T cell engager could redirect T lymphocytes´ cytotoxicity towards Gb3-expressing lymphoma-derived cells.

The potential of rationally engineered lectins to produce lectibodies has been already investigated in several studies in the past few years [104]. Through the genetic fusion of a lectin and an antibody´s crystallizable fragment (Fc) of immunoglobulin G (IgG), the resulting lectibody molecules have shown potential as antiviral proteins. The recognition of carbohydrates on the envelope of viruses by the lectin domain, coupled to the antibody effector functions of the Fc fragment such as complement-dependent cytotoxicity (CDC), antibody-dependent cell-mediated cytotoxicity (ADCC) or antibody-dependent cell-mediated phagocytosis (ADCP) have led to successful neutralization of viral entry into host cells and clearance of cells infected by viruses [105]. Our new Stx1B-scFv OKT3 lectibody resembles the previously described lectibodies as it combines a lectin with an antibody fragment, nevertheless, the architecture is quite different. In lieu of the Fc fragment, we employed the scFv OKT3 as a T cell engager and selectively conjugated it to the Gb3-binding Stx1B lectin instead of genetically fusing it. This approach allowed us to select the attachment points for maximum functionality of both components and to join them with a predefined spacing using linker molecules. The lectin Stx1B was selected to successfully recognize Gb3-expressing tumors as previously described [18, 44–47]. Due to the invariant property of CD3 chains in the TCR [106], CD3 was here chosen as a T cell surface target for the lectibody. The monoclonal antibody OKT3 recognizes a region of the antigenic CD3ε on human T cells and induces an immune response by T cell activation and proliferation [107]. Full-length antibodies can be produced in *E. coli* [108–110]. However, the balanced expression of the heavy- and light chains constituting the large antibody molecule, which requires several correctly formed disulfide bonds for its functional folding, seriously challenges the prokaryotic host [111]. Moreover, antibodies produced in *E. coli* are not glycosylated, which can affect their stability [112]. For these reasons, *E. coli* has been used to produce antibody fragments such as Fabs and scFvs rather than full-length antibodies. In this study, we employed the OKT3 single chain variable fragment because it readily binds to the CD3 antigen, is stable and efficiently produced in *E. coli* [86, 113].

These properties render scFv OKT3 an excellent candidate as the T cell engager component of the lectibody. To crosslink Gb3-expressing tumor cells with T cells via CD3 of the TCR, the lectin Stx1B and the scFv OKT3 must be physically linked. The linkage can be affected at the gene level or by chemical ligation on the protein level. In general, genetic fusions open a narrow window for conjugating proteins either on the N-terminus or on the C-terminus. The approach leaves no room for site-selective conjugations, offers only limited options for linkers and poses limitations when the biological activity of one (or both) of the fusion partners depends on the free terminus [114]. Nevertheless, gene fusions such as of human α-L-iduronidase on the N-terminus of RTB lectin [115] and the F_c region of human IgG1 to the C-terminus of Avaren lectin [105] were previously demonstrated as functional drug delivery systems. Fucose binding rBC2LCN lectin fused to pseudomonas exotoxin A proved effective in colorectal cancer treatment [116]. Linkage at the protein level is often realized by chemical ligations involving lysine- and cysteine residues in proteins. Yet, more than one lysine or cysteine in the protein sequence will spoil the regioselectivity [117]. The conjugation reactions are inefficient if the lysine- or cysteine residues are buried in the protein structure [118]. A few chemically conjugated lectin-drug delivery vehicles were tested as potential biotherapeutics. For instance, wheat germ agglutinin (WGA)-conjugated liposomes loaded with amoxicillin showed potent antimicrobial activity [119]. To overcome the above-mentioned limitations of genetic fusions and bioconjugation at canonical amino acids such as lysine and cysteine, we embarked on a bioorthogonal conjugation strategy for Stx1B and the scFv OKT3. Bioorthogonal conjugation exploits unique reactive groups that are installed at predefined positions in the protein conjugation partners. To site-selectively install the unique reactivity, ncAAs carrying a corresponding reactive side chain can be introduced into the target protein(s) at an in-frame amber stop codon [117]. Here we used the pyrrolysyl-tRNA synthetase from *Methanosarcina mazei* and its cognate amber suppressor *Mm*$tRNA_{CUA}$ for this purpose. The *Mm*PylRS/*Mm*$tRNA_{CUA}$ pair is orthogonal in *E. coli*, which means that the *Mm*PylRS does not charge any of the *E. coli* tRNAs, nor is the *Mm*$tRNA_{CUA}$ charged with a canonical amino acid by any of the host aminoacyl-tRNA synthetases. Wild-type *Mm*PylRS accepts a palette of (pyrol)lysine derivatives such as AzK [87]. We selected the sites for incorporation of AzK into Stx1B and scFv OKT3 such that the reactive azido-group would be surface exposed and as distant as possible from the glycan- or antigen-binding sites, respectively. These conditions were excellently fulfilled by residues K9 and E129 of Stx1B and scFv OKT3 (Fig. 1).

The direct bioorthogonal conjugation of two proteins requires that they are functionalized with compatible reactive groups. Unless an orthogonal pair accepts both corresponding ncAAs, individual orthogonal pairs are necessary [87]. Orthogonal pairs for the incorporation of azido-ncAAs [87, 120], cyclooctynyllysine derivatives [121], ncAAs with *trans*-cyclooctene- and bicyclooctyne- [122] as well as tetrazine- [123] side chain moieties were previously devised. While the azido-ncAAS such as AzK and *para*-azido-L-phenylalanine can be purchased, the ncAAs with reactive handles for SPAAC or IEDDA are either extremely expensive or commercially unavailable, which severely limits their use in a biotechnology lab. Being confronted with these issues, we decided to take an alternative path. Instead of directly linking Stx1B and scFv OKT3 *via* compatible reactive groups for SPAAC or IEDDA, we embarked on a two-step strategy (Fig. 3a): We first functionalized both proteins with an azido-group by the site-specific

incorporatin of AzK as outlined above. AzK was efficiently incorporated into scFv OKT3 and Stx1B as reflected by titers corresponding to 70 % and 93 % of the corrspondingwild-type proteins. The azide groups allowed us to perform a SPAAC reaction with bi-functional linker molecules that carried each an azide-reactive DBCO group on the one end and a *trans*-cyclooctyne- or a tetrazine-moiety for IEDDA on the other. The resulting methyltetrazine functionalized Stx1B K9Tz and *trans*-cyclooctene functionalized scFv OKT3 E129TCO spontaneously assembled into the Stx1B-scFv OKT3 lectibody in the second conjuagtion step. Since the conjugate would be used for cell assays and to avoid copper-induced toxic effects in cell lines [124], we did not consider copper(I)-catalyzed azide-alkyne cycloaddition (CuAAC) for the first-step conjugations [125]. Besides employing the commercially available SPAAC-reactive AzK that can be efficiently incorporated into target proteins, the two-step conjugation strategy offered another benefit. Selecting the linker lengths allowed flexibility in the orientation of Stx1B and scFv OKT3 in the Stx1B-scFv OKT3 conjugate such that the bispecific properties were retained. This flexibility is particularly crucial for the conjugation of large molecules such as proteins. Our prediction of the lectibody structure suggested that this would be the case. Indeed, the flow cytometry analysis confirmed that the Stx1B and scFv OKT3 modules preserved their affinity and recognition towards Gb3 and CD3 antigens, respectively, upon conjugation. Moreover, we observed the selective killing of Gb3-expressing cancer cells, which indicates that the T cells were brought in close contact with the cancer cells.

While the structural prediction of the lectibody indicated that five scFv OKT3 molecules can be conjugated to a Stx1B pentamer, our SEC results showed that only three scFv OKT3 molecules were conjugated (Table S3). This result adds another hint to the fact that bioorthogonal conjugation efficiencies rarely derive a 100% conjugate yield. Varying conjugation efficiencies were reported previously even with small molecules such as fluorescein and with DNA oligomers. For instance, Synakewicz et al. reported 47% yield for conjugating proteins with azide-modified DNA oligomers by SPAAC [76], and Maggi et al. observed a remarkable 62 % onjugation of trastuzumab-tetrazine with TCO-fluorescein by the IEDDA reaction [126]. These findings illustrate that conjugation efficiencies vary not only with the conjugation partners, i.e. protein with small molecule or DNA oligomer, but also with the conjugation method used. In this study, we were able to successfully conjugate three large ~ 30 kDa scFv OKT3 molecules to one ~ 45 kDa Stx1B pentamer *via* linkers by two successive SPAAC and IEDDA click reactions. Although studies by Li et al. [127] observed reduced cytotoxicity with the linker-based drug conjugate, our linker-based lectibody mediated crosslinking of T cells to tumor cells and induced high specific killing. As demonstrated, the Stx1B-scFv OKT3 promotes up to 93% of Burkitt´s lymphoma-derived tumor cells elimination within 48 hours of treatment. Strikingly, low nanomolar concentrations (7 nM and 35.6 nM) of the lectibody induced a potent T cells response against $Gb3^+$ Ramos cells and promoted $CD8^+$ T cells activation. On the one hand, linkers aid in the flexible orientation of the conjugated proteins and, on the other hand, they cause non-specific interactions leading to low yields during conjugation due to their hydrophobicity as reported elsewhere [128, 129]. It is key to understand what role the hydrophopathy of the linkers plays in the conjugation reaction to tackle the incomplete decoration of the Stx1B pentamer with the scFv OKT3 modules. For instance, Rahim et al. showed that 90% of the TCO groups without a linker attached on the surface of monoclonal antibodies were masked by their

hydrophobic interactions with the antibodies. They had overcome this problem by adding hydrophilic PEG to the linker between the reactive groups [128]. In the similar way, to improve the conjugation efficiency of Stx1B with scFv OKT3 in the future, water-soluble methyltetrazine-PEG-DBCO linkers of short varying lengths might be used to reduce non-specific interactions.

Noticeably, the Stx1B-scFv OKT3 lectibody did not affect the viability of Gb3 Namalwa cells, excluding the presence of undesired off-target cytotoxicity. The observed poor unspecific binding to off-targets by linker-based drug conjugates are in line with Li et al. [127]. To this matter, the excellent specificity of BiTEs has made this platform an exquisite system for treating cancer. Due to their bispecific configuration, the induction of a strong T cell response is accomplished by physically bridging cells, and the linkage of T cells to tumor cells is crucial to the BiTE´s cytotoxic mechanism. Single-sided binding of BiTE molecules is not sufficient in driving the activation of T cells [130], nor to induce cytokines expression – including interferon gamma, tumor necrosis factor alpha, IL-6, and IL-10 – that are upregulated upon T cells stimulation. Lack of dual binding, as proven for Gb3 Namalwa cells, demonstrated the ability of Stx1B-scFv OKT3 to circumvent undesired T cell activation. This finding suggests the strict dependence of this lectibody on simultaneous T cell-tumor cell engagement, only in the presence of the GSL Gb3.

According to SEC analysis, the purified lectibody consisted of a conjugate of 140 kDa in size. This lectibody is roughly three times bigger in size than other recombinant bispecific antibodies able to redirect T lymphocytes to tumor cells. Generally, most bispecific antibody platforms – including BiTEs, tandem scFv molecules (taFv), diabodies (Db), or single chain diabodies (scDb) [131–133] – consist of small molecules with molecular masses of 50–60 kDa. However, due to their small size, these formats often suffer from poor pharmacokinetic (PK) and pharmacodynamic (PD) properties *in vivo*. For example, they are rapidly cleared from circulation and their half-life is less than 30 minutes, which makes it difficult to target them to the site-of-action for long duration times [134–136]. This trait hampers their therapeutic applications, as they require multiple doses and repeated injections or infusions of treatment. Several antibody-based platforms have been engineered to improve their PK properties, and most attempts have been directed so far to increase their molecular sizes. The addition of a third scFv to the polypeptide chain of bispecific antibodies led to the design of single chain triplebody formats (sctbs) with a mass of about 90 kDa, exhibiting one domain for the recruitment of effector cells and two specific binding sites for antigens on tumor cells [137]. Such design intended to promote a bivalent binding of cancer cells, thus targeting low-density tumor antigens, and a prolonged half-life of the format, whose molecular size was above the kidney exclusion limit. Several sctb prototypes were tested and published, and potent lysis of CD19-positive lymphoma cells and acute myeloid leukemia cells was reported [138–140]. The trispecific arrangement of the recombinant antibody showed favorable features in cell culture as well as in mice, redirecting the cytotoxicity of $CD16^+$ effector cells towards $CD19^+$, $CD123^+$, $CD33^+$ tumor cells and doubling the serum half-life as a consequence of the increased mass. Other common strategies comprise chemical coupling of polyethylene glycol (PEG) chains [141], multimerization design [135, 142], or fusion with long-circulating serum proteins such as albumin [143, 144]. Due to its larger size, the Stx1B-scFv OKT3 lectibody presented in this study has a great potential to avoid clearance from serum

within few hours. To this end, future *in vivo* studies are required to establish the clearance rate and renal excretion of Stx1B-scFv OKT3, assessing the lectibody´s circulation times and protection from catabolism. On the other end, potential off-target cytotoxicity should be evaluated as a consequence of the lectibody persistence and recirculation in plasma. This includes the induction of T cell-mediated lysis in cells and tissues which present only a mild expression of this GSL, and the overactivation of the immune system after a stable binding of the scFv OKT3 to CD3 receptors on the surface of $CD4^+$ and $CD8^+$ T cells.

The remarkable performance of the Stx1B-scFv OKT3 lectibody in enabling T cell-mediated lysis of tumor cells is accompanied by activation of the cytotoxic $CD8^+$ T lymphocytes. The treatment elicited a notable upregulation of crucial markers at the surface of T cells – namely CD69, CD71, and CD25 – at 24 and 48 hours post-treatment. The appearance of such activation markers led to the identification of different stages in the T cells activation process, which was exclusively driven by the co-presence of lectibody and $Gb3^+$ target cells. CD69, CD71 and CD25 were significantly increased and reached a peak in surface expression that overlaps with the onset of cytotoxic activity, precisely at 24 and 48 hours. This increment in expression was elicited solely when $Gb3^+$ Ramos cells and Stx1B-scFv OKT3 were added to the culture, indicating the simultaneous engagement of effector and target cells and the target-specific killing induced by our treatment. These findings are in line with the therapeutic mechanism of action reported for BiTEs. Accordingly, a unique feature of BiTE-induced T cell activation is the lack of dependence upon T cell co-stimulation. Several studies of BiTEs with various specificity have demonstrated that these molecules induce significant cytotoxicity by T cells in the absence of co-stimulation, such as through anti-CD28 antibodies and IL-2 [130, 145].

Bifunctional molecules represent a promising anti-cancer arsenal, targeting a variety of tumor-associated antigens on both solid and hematologic tumors [63]. In a combinatorial approach, our lectibody might improve the outcome of existing therapies for the eradication of those tumor cells which present dramatic alterations of glycosylation at the surface. When targeting cancer-associated glycans, glycan-binding proteins (GBPs), such as lectins and anti-glycan antibodies, can be used to discriminate between tumor and normal cells. As tumor-targeting ligands, lectins can be used to increase the selectivity and efficacy of anti-cancer treatments and enhance their concentration at the tumor sites. Interestingly, in addition to Stx1B, several other bacterial lectins have found application in tumor detection or treatment. For example, the cholera toxin (Ctx) from *Vibrio cholerae*, belonging to the AB_5 family of microbial toxins, has been proven effective in a number of studies for tumor targeting and imaging [38]. The affinity for the ganglioside GM1, which is highly expressed in the blood-brain barrier, resulted in the investigation of its B-subunit (CtxB) for new anti-glioma chemotherapy strategies, where CtxB nanoparticles loaded with paclitaxel induced apoptosis of intracranial glioma cells *in vivo* and extended survival in mice models [146]. At the same time, this lectin was reported to be highly efficient in sensitive retrograde neuronal tracing [147–150]. More recently, we demonstrated the efficiency of the engineered FS-Janus lectin consisting of two carbohydrate-binding domains in detecting and targeting pathological hypersialylation on non-small cell lung cancer *via* its multivalent architecture, and with remarkable nanomolar avidity

[151, 152]. The chimeric, bispecific lectin was reported to crosslink glyco-decorated giant unilamellar vesicles and lung epithelial tumor cells, leading to the intracellular uptake of liposomal content and unraveling its potential in lectin-mediated drug delivery. Moreover, Meléndez et al. developed a panel of lectin-based chimeric antigen receptors (CARs) T cells, which demonstrated high therapeutical potential towards a variety of hematological malignancies and solid tumors expressing Gb3. In their studies, the Gb3-binding lectins StxB from *Shigella dysenteriae*, LecA from *Pseudomonas aeruginosa*, and the engineered Mitsuba from *Mytilus galloprovincialis* were employed to recognize the TACA Gb3 and fused to a second-generation CAR, achieving excellent target-specific cytotoxicity against Burkitt's lymphoma-derived cell lines as well as colorectal and triple-negative breast-cancer [153]. Overall, these studies together with our current study support the potential of lectins as tools in many therapeutical applications where the glycome plays a crucial role in the development and sustainment of pathological conditions.

The described observations of dual-binding dependence, target-specific killing and absence of co-stimulation suggest a model for our lectibody-mediated cytotoxicity, where multiple lectibody-dependent binding events occur between T cells and tumor cells in culture, promoting clustering of T cell receptors and activation of cytotoxic signaling. Indeed, the presence of several scFvs OKT3 in the lectibody allows this bispecific T cell engager to be presented in a polyvalent form. This might induce the formation of an immunological synapse and release of cytolytic granules resulting in tumor cell lysis, as observed for BiTEs. There is much further knowledge to gain regarding the mechanism of action of the lectibody. Foremost, the investigation of its efficacy and potency in animal models must be carried out to further characterize the potential of this bispecific format in cancer therapy, as well as a better understanding of how the lectibody is processed by the body and of the side effects that might appear during therapy. In addition, examining Stx1B-scFv OKT3 in combination with other therapies will be necessary. For instance, it will be interesting to see how the lectibody performs in association with immune checkpoint inhibitors, which promote a greater T cell activation. A combinatorial strategy of this type could increase Stx1B-scFv OKT3 efficacy by enhancing and maintaining T cell activity for tumor eradication [154]. As with most new immunotherapies, it would be attractive to examine if this lectibody is clinically useful against solid malignancies, and whether its performance can overcome the challenges imposed by the tumor microenvironment. Nevertheless, it is important to point out that the GSL Gb3 is present on the cell membrane of a variety of non-transformed cells, which could lead to the onset of off-target cytotoxicity upon administration of the lectibody. A key factor that must be taken into account is the difference in Gb3 expression levels between pathological and physiological states, highlighted by the impact they have on StxB participation to receptor recognition [155–158]. It has been proven that the binding of the toxin and its targeting to a specific intracellular transport pathway within $Gb3^+$ cells is determined by the heterogeneity in Gb3 isoforms and the abundance of Gb3 in the lipid rafts of the plasma membrane [159]. According to these studies, Melendez et al. correlated the cytotoxicity of Gb3-targeting CAR T cells towards distinct $Gb3^+$ and Gb3 cells lines with Gb3 abundance and isoform variations *via* mass spectrometry analysis [153]. The analysis revealed a strong dependency between Gb3 presence and structural variability and specific killing by the lectin-CAR T cells. Ultimately, it becomes evident the

necessity for a screening of cytological specimens to determine the Gb3 status of patients prior to making such a therapeutic choice.

Finally, the lectibody concept described here possesses versatile features, since it can be adapted to other TACAs by exchanging Stx1B with another lectin. Recent advances in the use of lectins in research and medicine suggest they are potential tools for many applications, such as drug delivery and selective targeting of pathological conditions with a focus on glycosylation changes [49, 50]. Lectins engineering, as proven in this study, may offer the possibility to target glycan epitopes on tumor cells and boost the efficacy of current tumor therapies.

Conclusions

To summarize, our findings show a prospective proof-of-concept for lectin-induced T cell cytotoxicity towards malignant cells. A prototype of a lectibody with bifunctional properties was produced using a click conjugation strategy and its functionality was evaluated in cell-binding and cytotoxicity assays. Although the mechanism of action of Stx1B-scFv OKT3 has to be further explored *in vivo*, we demonstrate encouraging properties of a bispecific lectin-based platform that selectively targets altered glycostructures on tumor cells. Additional improvements will focus on the evaluation of linkers with increased length and longer incubation times of click reactions to optimize product yield. Nonetheless, the lectibody format represents a promising tool for cancer therapy and could enhance selective targeting of the glycome in many human malignancies.

Abbreviations

ADCs	Antibody-drug conjugates
AzK	Azidolysine
BiTEs	Bispecific T cell Engagers
BLA	Burkitt’s lymphoma-associated antigen
BLI	Bioluminescence
bsAbs	Bispecific antibodies
CTLs	Cytotoxic T lymphocytes
DBCO	Dibenzocyclooctyne
DMEM	Dulbecco's Modified Eagle Medium
E:T	Effector to target

FACS	Fluorescence-activated cell sorting
Gb3	Globotriaosylceramide
GCS	Glucosylceramide synthase
GSL	Glycosphingolipid
IEDDA	Inverse Electron Demand Diels-Alder
mAb	Monoclonal antibody
MFI	Mean fluorescence intensity
ncAA	Non-canonical amino acid
PBMC	Peripheral blood mononuclear cell
PBS	Phosphate-buffered saline
PDB	Protein data bank
PEG	Polyethylene glycol
PPMP	1-phenyl-2-palmitoylamino-3-morpholino-1-propanol
RLU	Relative light units
RPMI	Roswell Park Memorial Institute
scFv	Single chain variable fragment
SDS-PAGE	Sodium dodecyl sulfate–polyacrylamide gel electrophoresis
SPAAC	Strain-Promoted Azide-Alkyne Cycloaddition
Stx1B	Shiga toxin 1 B-subunit
TAA	Tumor-associated antigen
TACA	Tumor-associated carbohydrate antigen
TCR	T cell receptor

Declarations

Supplementary Information

The online version contains supplementary material available.

Authors´ contributions

Conception and design of the research: FR, RP, BW, WR; funding acquisition: BW, WR; investigation: FR, RP; methodology: JT, AVM, DK, ONM; supervision: BW, WR; writing—original draft: FR, RP; writing—review and editing: JT, AVM, DK, ONM, BW, WR. All authors agreed on the final version of the manuscript.

Funding

This research was funded by the European Union's Horizon 2020 Research and Innovation Program under the Marie Skłodowska-Curie grant agreement synBIOcarb (No. 814029). Moreover, WR acknowledges support by the Deutsche Forschungsgemeinschaft (DFG, German Research Foundation) under Germany's Excellence Strategy (GSC-4, EXC-294 and EXC-2189) and the German Research Foundation grant Major Research Instrumentation (project number: 438033605), by the Ministry for Science, Research and Arts of the State of Baden-Württemberg (Az: 33-7532.20; and partial funding of SGBM PhD thesis), and by the Freiburg Institute for Advanced Studies (FRIAS). This publication is partially based upon work from COST Action CA18103 (INNOGLY), supported by COST (European Coorperation in Science and Technology). ONM thanks the financial support from the government assignment for FRC Kazan Scientific Center of RAS. In addition, we would like to express our gratitude to the Life Imaging Center (LIC) of the University of Freiburg for support.

Acknowledgements

We thank the Blood Donation Center, Medical Centre of the University of Freiburg for providing LRS chambers. We also express gratitude to Dr. Pavel Salavei of the CIBSS Signaling Factory, University of Freiburg, Germany, for his help and guidance in flow cytometry. Barbara Darnhofer and Ruth Birner-Grünberger as well as the BOKU Core Facility Mass Spectrometry are acknowledged for excellent support with mass spectrometry.

Data availability

The datasets generated and/or analyzed during the current study are available from the corresponding authors on reasonable request.

Compliance with ethical standards

Conflict of interest

The authors declare no conflict of interest.

Ethics approval

LRS chambers used as blood sources were purchased from the blood bank of the University Medical Centre Freiburg (approval of the University Freiburg Ethics Committee: 147/15).

Consent for publication

Not applicable.

References

1. Ferlay J, Ervik M, Lam F, et al (2020) Global Cancer Observatory: Cancer Today. In: Lyon: International Agency for Research on Cancer; 2020 (https://gco.iarc.fr/today, accessed February 2021)
2. Peixoto A, Relvas-Santos M, Azevedo R, et al (2019) Protein Glycosylation and Tumor Microenvironment Alterations Driving Cancer Hallmarks. Frontiers in Oncology 9:. https://doi.org/10.3389/fonc.2019.00380
3. Pinho SS, Reis CA (2015) Glycosylation in cancer: mechanisms and clinical implications. Nature Reviews Cancer 15:540–555. https://doi.org/10.1038/nrc3982
4. Reis CA, Osorio H, Silva L, et al (2010) Alterations in glycosylation as biomarkers for cancer detection. Journal of Clinical Pathology 63:322–329. https://doi.org/10.1136/jcp.2009.071035
5. Munkley J, Elliott DJ (2016) Hallmarks of glycosylation in cancer. Oncotarget 7:35478–89. https://doi.org/10.18632/oncotarget.8155
6. Varki A, Kannagi R, Toole BP (2009) Glycosylation Changes in Cancer. . In: Essentials of Glycobiology. , 2nd edition. Cold Spring Harbor (NY): Cold Spring Harbor Laboratory Press, New York
7. Rodrigues JG, Balmaña M, Macedo JA, et al (2018) Glycosylation in cancer: Selected roles in tumour progression, immune modulation and metastasis. Cellular Immunology 333:46–57. https://doi.org/10.1016/j.cellimm.2018.03.007
8. Hakomori S (1984) Tumor-Associated Carbohydrate Antigens. Annual Review of Immunology 2:103–126. https://doi.org/10.1146/annurev.iy.02.040184.000535
9. Costa AF, Campos D, Reis CA, Gomes C (2020) Targeting Glycosylation: A New Road for Cancer Drug Discovery. Trends in Cancer 6:757–766. https://doi.org/10.1016/j.trecan.2020.04.002
10. Hakomori S-I, Zhang Y (1997) Glycosphingolipid antigens and cancer therapy. Chemistry & Biology 4:97–104. https://doi.org/10.1016/S1074-5521(97)90253-2
11. Wiels J, Fellous M, Tursz T (1981) Monoclonal antibody against a Burkitt lymphoma-associated antigen. Proceedings of the National Academy of Sciences 78:6485–6488. https://doi.org/10.1073/pnas.78.10.6485
12. LaCasse E, Saleh M, Patterson B, et al (1996) Shiga-like toxin purges human lymphoma from bone marrow of severe combined immunodeficient mice. Blood 88:1561–1567. https://doi.org/10.1182/blood.V88.5.1561.bloodjournal8851561
13. LaCasse EC, Bray MR, Patterson B, et al (1999) Shiga-like toxin-1 receptor on human breast cancer, lymphoma, and myeloma and absence from CD34(+) hematopoietic stem cells: implications for ex

vivo tumor purging and autologous stem cell transplantation. Blood 94:2901–10

14. Johansson D, Kosovac E, Moharer J, et al (2009) Expression of verotoxin-1 receptor Gb3 in breast cancer tissue and verotoxin-1 signal transduction to apoptosis. BMC Cancer 9:67. https://doi.org/10.1186/1471-2407-9-67
15. Arab S, Russel E, Chapman WB, et al (1997) Expression of the verotoxin receptor glycolipid, globotriaosylceramide, in ovarian hyperplasias. Oncol Res 9:553–63
16. Kovbasnjuk O, Mourtazina R, Baibakov B, et al (2005) The glycosphingolipid globotriaosylceramide in the metastatic transformation of colon cancer. Proceedings of the National Academy of Sciences 102:19087–19092. https://doi.org/10.1073/pnas.0506474102
17. Falguières T, Maak M, von Weyhern C, et al (2008) Human colorectal tumors and metastases express Gb_3 and can be targeted by an intestinal pathogen-based delivery tool. Molecular Cancer Therapeutics 7:2498–2508. https://doi.org/10.1158/1535-7163.MCT-08-0430
18. Maak M, Nitsche U, Keller L, et al (2011) Tumor-Specific Targeting of Pancreatic Cancer with Shiga Toxin B-Subunit. Molecular Cancer Therapeutics 10:1918–1928. https://doi.org/10.1158/1535-7163.MCT-11-0006
19. Distler U, Souady J, Hülsewig M, et al (2009) Shiga Toxin Receptor Gb3Cer/CD77: Tumor-Association and Promising Therapeutic Target in Pancreas and Colon Cancer. PLoS ONE 4:e6813. https://doi.org/10.1371/journal.pone.0006813
20. Hakomori S (1981) Glycosphingolipids in Cellular Interaction, Differentiation, and Oncogenesis. Annual Review of Biochemistry 50:733–764. https://doi.org/10.1146/annurev.bi.50.070181.003505
21. Schnaar RL, Kinoshita T (2015) Glycosphingolipids
22. Lingwood CA, Binnington B, Manis A, Branch DR (2010) Globotriaosyl ceramide receptor function - Where membrane structure and pathology intersect. FEBS Letters 584:1879–1886. https://doi.org/10.1016/j.febslet.2009.11.089
23. Eierhoff T, Bastian B, Thuenauer R, et al (2014) A lipid zipper triggers bacterial invasion. Proceedings of the National Academy of Sciences 111:. https://doi.org/10.1073/pnas.1402637111
24. Omidvar R, Ayala YA, Brandel A, et al (2021) Quantification of nanoscale forces in lectin-mediated bacterial attachment and uptake into giant liposomes. Nanoscale 13:4016–4028. https://doi.org/10.1039/D0NR07726G
25. Siukstaite L, Imberty A, Römer W (2021) Structural Diversities of Lectins Binding to the Glycosphingolipid Gb3. Frontiers in Molecular Biosciences 8:. https://doi.org/10.3389/fmolb.2021.704685
26. Juillot Samuel, Römer Winfried (2014) Shiga Toxins. In: Stefano Morabito (ed) Pathogenic Escherichia coli: Molecular and Cellular Microbiology. Caister Academic Press, EU Reference Laboratory for E. coli, Veterinary Public Health and Food Safety Department, Istituto Superiore di Sanità, Rome, Italy, pp 79–101

27. Kociurzynski R, Makshakova ON, Knecht V, Römer W (2021) Multiscale Molecular Dynamics Studies Reveal Different Modes of Receptor Clustering by Gb3-Binding Lectins. Journal of Chemical Theory and Computation 17:2488–2501. https://doi.org/10.1021/acs.jctc.0c01145
28. Schubert T, Sych T, Madl J, et al (2020) Differential recognition of lipid domains by two Gb3-binding lectins. Scientific Reports 10:9752. https://doi.org/10.1038/s41598-020-66522-8
29. Eierhoff T, Stechmann B, Römer W (2012) Pathogen and Toxin Entry - How Pathogens and Toxins Induce and Harness Endocytotic Mechanisms. In: Molecular Regulation of Endocytosis. InTech
30. Smith D, Lord J, Roberts L, Johannes L (2004) Glycosphingolipids as toxin receptors. Seminars in Cell & Developmental Biology 15:397–408. https://doi.org/10.1016/j.semcdb.2004.03.005
31. Zheng S, Eierhoff T, Aigal S, et al (2017) The Pseudomonas aeruginosa lectin LecA triggers host cell signalling by glycosphingolipid-dependent phosphorylation of the adaptor protein CrkII. Biochimica et Biophysica Acta (BBA) - Molecular Cell Research 1864:1236–1245. https://doi.org/10.1016/j.bbamcr.2017.04.005
32. Brandel A, Aigal S, Lagies S, et al (2021) The Gb3-enriched CD59/flotillin plasma membrane domain regulates host cell invasion by Pseudomonas aeruginosa. Cellular and Molecular Life Sciences 78:3637–3656. https://doi.org/10.1007/s00018-021-03766-1
33. Conradi H (1903) Ueber lösliche, durch aseptische Autolyse erhaltene Giftstoffe von Ruhr- und Typhusbazillen. DMW - Deutsche Medizinische Wochenschrift 29:26–28. https://doi.org/10.1055/s-0028-113822834.
34. Karch H, Tarr PI, Bielaszewska M (2005) Enterohaemorrhagic Escherichia coli in human medicine. Int J Med Microbiol 295:405–18. https://doi.org/10.1016/j.ijmm.2005.06.009
35. Kovbasnjuk O (2005) New insights into the role of Shiga toxins in intestinal disease. Gastroenterology 129:1354–1355. https://doi.org/10.1053/j.gastro.2005.08.032
36. Tarr PI, Gordon CA, Chandler WL (2005) Shiga-toxin-producing Escherichia coli and haemolytic uraemic syndrome. The Lancet 365:1073–1086. https://doi.org/10.1016/S0140-6736(05)71144-2
37. Jackson MP, Newland JW, Holmes RK, O'Brien AD (1987) Nucleotide sequence analysis of the structural genes for Shiga-like toxin I encoded by bacteriophage 933J from Escherichia coli. Microbial Pathogenesis 2:147–153. https://doi.org/10.1016/0882-4010(87)90106-9
38. Danielewicz N, Rosato F, Dai W, et al (2022) Microbial carbohydrate-binding toxins – From etiology to biotechnological application. Biotechnology Advances 59:107951. https://doi.org/10.1016/j.biotechadv.2022.107951
39. Lingwood C (1996) Role of verotoxin receptors in pathogenesis. Trends in Microbiology 4:147–153. https://doi.org/10.1016/0966-842X(96)10017-2
40. Römer W, Berland L, Chambon V, et al (2007) Shiga toxin induces tubular membrane invaginations for its uptake into cells. Nature 450:670–675. https://doi.org/10.1038/nature05996
41. Windschiegl B, Orth A, Römer W, et al (2009) Lipid Reorganization Induced by Shiga Toxin Clustering on Planar Membranes. PLoS ONE 4:e6238. https://doi.org/10.1371/journal.pone.0006238

42. Johannes L, Römer W (2010) Shiga toxins — from cell biology to biomedical applications. Nature Reviews Microbiology 8:105–116. https://doi.org/10.1038/nrmicro2279
43. Odumosu O, Nicholas D, Yano H, Langridge W (2010) AB Toxins: A Paradigm Switch from Deadly to Desirable. Toxins (Basel) 2:1612–1645. https://doi.org/10.3390/toxins2071612
44. El Alaoui A, Schmidt F, Amessou M, et al (2007) Shiga Toxin-Mediated Retrograde Delivery of a Topoisomerase I Inhibitor Prodrug. Angewandte Chemie International Edition 46:6469–6472. https://doi.org/10.1002/anie.200701270
45. Distler U, Souady J, Hülsewig M, et al (2009) Shiga Toxin Receptor Gb3Cer/CD77: Tumor-Association and Promising Therapeutic Target in Pancreas and Colon Cancer. PLoS ONE 4:e6813. https://doi.org/10.1371/journal.pone.0006813
46. Geyer PE, Maak M, Nitsche U, et al (2016) Gastric Adenocarcinomas Express the Glycosphingolipid Gb_3/CD77: Targeting of Gastric Cancer Cells with Shiga Toxin B-Subunit. Molecular Cancer Therapeutics 15:1008–1017. https://doi.org/10.1158/1535-7163.MCT-15-0633
47. Batisse C, Dransart E, Ait Sarkouh R, et al (2015) A new delivery system for auristatin in STxB-drug conjugate therapy. European Journal of Medicinal Chemistry 95:483–491. https://doi.org/10.1016/j.ejmech.2015.03.047
48. Distler U, Souady J, Hülsewig M, et al (2009) Shiga Toxin Receptor Gb3Cer/CD77: Tumor-Association and Promising Therapeutic Target in Pancreas and Colon Cancer. PLoS ONE 4:e6813. https://doi.org/10.1371/journal.pone.0006813
49. S. Coulibaly F, C. Youan B-B (2017) Current status of lectin-based cancer diagnosis and therapy. AIMS Molecular Science 4:. https://doi.org/10.3934/molsci.2017.1.1
50. Müller SK, Wilhelm I, Schubert T, et al (2017) Gb3-binding lectins as potential carriers for transcellular drug delivery. Expert Opinion on Drug Delivery 14:. https://doi.org/10.1080/17425247.2017.1266327
51. Mody R, Joshi SH antaram, Chaney W (1995) Use of lectins as diagnostic and therapeutic tools for cancer. Journal of Pharmacological and Toxicological Methods 33:. https://doi.org/10.1016/1056-8719(94)00052-6
52. Bies C, Lehr C-M, Woodley JF (2004) Lectin-mediated drug targeting: history and applications. Advanced Drug Delivery Reviews 56:. https://doi.org/10.1016/j.addr.2003.10.030
53. Dingjan T, Spendlove I, Durrant LG, et al (2015) Structural biology of antibody recognition of carbohydrate epitopes and potential uses for targeted cancer immunotherapies. Molecular Immunology 67:75–88. https://doi.org/10.1016/j.molimm.2015.02.028
54. Agostino M, Farrugia W, Sandrin MS, et al (2012) Structural Glycobiology of Antibody Recognition in Xenotransplantation and Cancer Immunotherapy. In: Anticarbohydrate Antibodies. Springer Vienna, Vienna, pp 203–228
55. Durrant LG, Noble P, Spendlove I (2012) Immunology in the clinic review series; focus on cancer: glycolipids as targets for tumour immunotherapy. Clinical and Experimental Immunology 167:206–215. https://doi.org/10.1111/j.1365-2249.2011.04516.x

56. Rabu C, McIntosh R, Jurasova Z, Durrant L (2012) Glycans as targets for therapeutic antitumor antibodies. Future Oncology 8:943–960. https://doi.org/10.2217/fon.12.88
57. Scott AM, Wolchok JD, Old LJ (2012) Antibody therapy of cancer. Nature Reviews Cancer 12:278–287. https://doi.org/10.1038/nrc3236
58. Chua JX, Durrant L (2017) Monoclonal Antibodies Against Tumour-Associated Carbohydrate Antigens. In: Carbohydrate. InTech
59. Rodrigues Mantuano N, Natoli M, Zippelius A, Läubli H (2020) Tumor-associated carbohydrates and immunomodulatory lectins as targets for cancer immunotherapy. Journal for ImmunoTherapy of Cancer 8:e001222. https://doi.org/10.1136/jitc-2020-001222
60. Weiner LM, Murray JC, Shuptrine CW (2012) Antibody-based immunotherapy of cancer. Cell 148:1081–4. https://doi.org/10.1016/j.cell.2012.02.034
61. Food and Drug Administration (2014) FDA Briefing Document. Oncologic Drugs Advisory Committee Meeting. BLA 125557 S-013 Blincyto (blinatumomab) Applicant: Amgen, Inc.
62. Lutterbuese R, Raum T, Kischel R, et al (2010) T cell-engaging BiTE antibodies specific for EGFR potently eliminate KRAS- and BRAF-mutated colorectal cancer cells. Proceedings of the National Academy of Sciences 107:12605–12610. https://doi.org/10.1073/pnas.1000976107
63. Huehls AM, Coupet TA, Sentman CL (2015) Bispecific T-cell engagers for cancer immunotherapy. Immunology & Cell Biology 93:290–296. https://doi.org/10.1038/icb.2014.93
64. Ali IU, Schriml LM, Dean M (1999) Mutational Spectra of PTEN/MMAC1 Gene: a Tumor Suppressor With Lipid Phosphatase Activity. JNCI Journal of the National Cancer Institute 91:1922–1932. https://doi.org/10.1093/jnci/91.22.1922
65. Sansal I, Sellers WR (2004) The Biology and Clinical Relevance of the *PTEN* Tumor Suppressor Pathway. Journal of Clinical Oncology 22:2954–2963. https://doi.org/10.1200/JCO.2004.02.141
66. Furman WL, Shulkin BL, Federico SM, et al (2017) Early response rates and Curie scores at end of induction: An update from a phase II study of an anti-GD2 monoclonal antibody (mAb) with chemotherapy (CT) in newly diagnosed patients (pts) with high-risk (HR) neuroblastoma (NB). Journal of Clinical Oncology 35:10534–10534. https://doi.org/10.1200/JCO.2017.35.15_suppl.10534
67. Lee J, Kim J, Kim S, et al (2017) P1.01-070 BIW-8962, an Anti-GM2 Ganglioside Monoclonal Antibody, in Advanced/Recurrent Lung Cancer: A Phase I/II Study. Journal of Thoracic Oncology 12:S1921–S1922. https://doi.org/10.1016/j.jtho.2017.09.724
68. Polonskaya Z, Savage PB, Finn MG, Teyton L (2019) High-affinity anti-glycan antibodies: challenges and strategies. Curr Opin Immunol 59:65–71. https://doi.org/10.1016/j.coi.2019.03.004
69. Amon R, Reuven EM, Leviatan Ben-Arye S, Padler-Karavani V (2014) Glycans in immune recognition and response. Carbohydrate Research 389:115–122. https://doi.org/10.1016/j.carres.2014.02.004
70. Kung PC, Goldstein G, Reinherz EL, Schlossman SF (1979) Monoclonal Antibodies Defining Distinctive Human T Cell Surface Antigens. Science (1979) 206:347–349. https://doi.org/10.1126/science.314668

71. Salmerón A, Sánchez-Madrid F, Ursa MA, et al (1991) A conformational epitope expressed upon association of CD3-epsilon with either CD3-delta or CD3-gamma is the main target for recognition by anti-CD3 monoclonal antibodies. J Immunol 147:3047–52
72. Galindo Casas M, Stargardt P, Mairhofer J, Wiltschi B (2020) Decoupling Protein Production from Cell Growth Enhances the Site-Specific Incorporation of Noncanonical Amino Acids in *E. coli*. ACS Synthetic Biology 9:3052–3066. https://doi.org/10.1021/acssynbio.0c00298
73. Tobola F, Sylvander E, Gafko C, Wiltschi B (2019) 'Clickable lectins': bioorthogonal reactive handles facilitate the directed conjugation of lectins in a modular fashion. Interface Focus 9:20180072. https://doi.org/10.1098/rsfs.2018.0072
74. Luo W-G, Liu H-Z, Lin W-H, et al (2013) Simultaneous splicing of multiple DNA fragments in one PCR reaction. Biological Procedures Online 15:9. https://doi.org/10.1186/1480-9222-15-9
75. Chan W-T, Verma CS, Lane DP, Gan SK-E (2013) A comparison and optimization of methods and factors affecting the transformation of *Escherichia coli*. Bioscience Reports 33:. https://doi.org/10.1042/BSR20130098
76. Synakewicz M, Bauer D, Rief M, Itzhaki LS (2019) Bioorthogonal protein-DNA conjugation methods for force spectroscopy. Scientific Reports 9:13820. https://doi.org/10.1038/s41598-019-49843-1
77. Chevallet M, Luche S, Rabilloud T (2006) Silver staining of proteins in polyacrylamide gels. Nature Protocols 1:1852–1858. https://doi.org/10.1038/nprot.2006.288
78. Gasteiger E, Hoogland C, Gattiker A, et al (2005) Protein Identification and Analysis Tools on the ExPASy Server. In: The Proteomics Protocols Handbook. Humana Press, Totowa, NJ, pp 571–607
79. Šali A, Blundell TL (1993) Comparative Protein Modelling by Satisfaction of Spatial Restraints. Journal of Molecular Biology 234:779–815. https://doi.org/10.1006/jmbi.1993.1626
80. Banks JL, Beard HS, Cao Y, et al (2005) Integrated Modeling Program, Applied Chemical Theory (IMPACT). Journal of Computational Chemistry 26:1752–1780. https://doi.org/10.1002/jcc.20292
81. Polak E, Ribiere G (1969) Note sur la convergence de méthodes de directions conjuguées. Revue française d'informatique et de recherche opérationnelle Série rouge 3:35–43. https://doi.org/10.1051/m2an/196903R100351
82. Hartl FA, Beck-Garcìa E, Woessner NM, et al (2020) Noncanonical binding of Lck to CD3ε promotes TCR signaling and CAR function. Nature Immunology 21:902–913. https://doi.org/10.1038/s41590-020-0732-3
83. Bio-Sharing.org Leukoreduction System (LRS) Chamber, platelet-only donor. In: https://bio-sharing.org/pdfs/Leukoreduction.pdf
84. Abe A, Inokuchi J, Jimbo M, et al (1992) Improved Inhibitors of Glucosylceramide Synthase1. The Journal of Biochemistry 111:191–196. https://doi.org/10.1093/oxfordjournals.jbchem.a123736
85. Melton-Celsa AR (2014) Shiga Toxin (Stx) Classification, Structure, and Function. Microbiology Spectrum 2:. https://doi.org/10.1128/microbiolspec.EHEC-0024-2013

86. Kipriyanov SM, Moldenhauer G, Martin AC, et al (1997) Two amino acid mutations in an anti-human CD3 single chain Fv antibody fragment that affect the yield on bacterial secretion but not the affinity. Protein Engineering Design and Selection 10:445–453. https://doi.org/10.1093/protein/10.4.445
87. Wan W, Tharp JM, Liu WR (2014) Pyrrolysyl-tRNA synthetase: An ordinary enzyme but an outstanding genetic code expansion tool. Biochimica et Biophysica Acta (BBA) - Proteins and Proteomics 1844:1059–1070. https://doi.org/10.1016/j.bbapap.2014.03.002
88. Gallegos KM, Conrady DG, Karve SS, et al (2012) Shiga Toxin Binding to Glycolipids and Glycans. PLoS ONE 7:e30368. https://doi.org/10.1371/journal.pone.0030368
89. Dommerholt J, Rutjes FPJT, van Delft FL (2016) Strain-Promoted 1,3-Dipolar Cycloaddition of Cycloalkynes and Organic Azides. Topics in Current Chemistry 374:16. https://doi.org/10.1007/s41061-016-0016-4
90. Knall A-C, Slugovc C (2013) Inverse electron demand Diels–Alder (iEDDA)-initiated conjugation: a (high) potential click chemistry scheme. Chemical Society Reviews 42:5131. https://doi.org/10.1039/c3cs60049a
91. Mangeney M, Richard Y, Coulaud D, et al (1991) CD77: an antigen of germinal center B cells entering apoptosis. European Journal of Immunology 21:1131–1140. https://doi.org/10.1002/eji.1830210507
92. Nudelman E, Kannagi R, Hakomori S, et al (1983) A Glycolipid Antigen Associated with Burkitt Lymphoma Defined by a Monoclonal Antibody. Science (1979) 220:509–511. https://doi.org/10.1126/science.6836295
93. Taga S, Carlier K, Mishal Z, et al (1997) Intracellular signaling events in CD77-mediated apoptosis of Burkitt's lymphoma cells. Blood 90:2757–67
94. Tétaud C, Falguières T, Carlier K, et al (2003) Two Distinct Gb3/CD77 Signaling Pathways Leading to Apoptosis Are Triggered by Anti-Gb3/CD77 mAb and Verotoxin-1. Journal of Biological Chemistry 278:45200–45208. https://doi.org/10.1074/jbc.M303868200
95. Smith-Garvin JE, Koretzky GA, Jordan MS (2009) T cell activation. Annu Rev Immunol 27:591–619. https://doi.org/10.1146/annurev.immunol.021908.132706
96. Cambiaggi C, Scupoli M, Cestari T, et al (1992) Constitutive expression of CD69 in interspecies T-cell hybrids and locus assignment to human chromosome 12. Immunogenetics 36:117–120. https://doi.org/10.1007/BF00215288
97. López-Cabrera M, Santis AG, Fernández-Ruiz E, et al (1993) Molecular cloning, expression, and chromosomal localization of the human earliest lymphocyte activation antigen AIM/CD69, a new member of the C-type animal lectin superfamily of signal-transmitting receptors. Journal of Experimental Medicine 178:537–547. https://doi.org/10.1084/jem.178.2.537
98. Reddy M, Eirikis E, Davis C, et al (2004) Comparative analysis of lymphocyte activation marker expression and cytokine secretion profile in stimulated human peripheral blood mononuclear cell cultures: an in vitro model to monitor cellular immune function. Journal of Immunological Methods 293:127–142. https://doi.org/10.1016/j.jim.2004.07.006

99. Salmerón A, Borroto A, Fresno M, et al (1995) Transferrin receptor induces tyrosine phosphorylation in T cells and is physically associated with the TCR zeta-chain. J Immunol 154:1675–83
100. Lum JB, Infante AJ, Makker DM, et al (1986) Transferrin synthesis by inducer T lymphocytes. Journal of Clinical Investigation 77:841–849. https://doi.org/10.1172/JCI112381
101. Jackson AL, Matsumoto H, Janszen M, et al (1990) Restricted expression of p55 interleukin 2 receptor (CD25) on normal T cells. Clinical Immunology and Immunopathology 54:126–133. https://doi.org/10.1016/0090-1229(90)90012-F
102. Zugazagoitia J, Guedes C, Ponce S, et al (2016) Current Challenges in Cancer Treatment. Clinical Therapeutics 38:1551–1566. https://doi.org/10.1016/j.clinthera.2016.03.026
103. Zhou S, Liu M, Ren F, et al (2021) The landscape of bispecific T cell engager in cancer treatment. Biomarker Research 9:38. https://doi.org/10.1186/s40364-021-00294-9
104. Nabi-Afjadi M, Heydari M, Zalpoor H, et al (2022) Lectins and lectibodies: potential promising antiviral agents. Cellular & Molecular Biology Letters 27:37. https://doi.org/10.1186/s11658-022-00338-4
105. Hamorsky KT, Kouokam JC, Dent MW, et al (2019) Engineering of a Lectibody Targeting High-Mannose-Type Glycans of the HIV Envelope. Molecular Therapy 27:2038–2052. https://doi.org/10.1016/j.ymthe.2019.07.021
106. Frank SJ, Samelson LE, Klausner RD (1990) The structure and signalling functions of the invariant T cell receptor components. Semin Immunol 2:89–97
107. Landegren U, Andersson J, Wigzell H (1984) Mechanism of T lymphocyte activation by OKT3 antibodies. A general model for T cell induction. European Journal of Immunology 14:325–328. https://doi.org/10.1002/eji.1830140409
108. Robinson M-P, Ke N, Lobstein J, et al (2015) Efficient expression of full-length antibodies in the cytoplasm of engineered bacteria. Nature Communications 6:8072. https://doi.org/10.1038/ncomms9072
109. Mazor Y, van Blarcom T, Mabry R, et al (2007) Isolation of engineered, full-length antibodies from libraries expressed in Escherichia coli. Nature Biotechnology 25:563–565. https://doi.org/10.1038/nbt1296
110. Simmons LC, Reilly D, Klimowski L, et al (2002) Expression of full-length immunoglobulins in Escherichia coli: rapid and efficient production of aglycosylated antibodies. Journal of Immunological Methods 263:133–147. https://doi.org/10.1016/S0022-1759(02)00036-4
111. Reilly DE, Yansura DG (2010) Production of Monoclonal Antibodies in E. coli. In: Current Trends in Monoclonal Antibody Development and Manufacturing. Springer New York, New York, NY, pp 295–308
112. Zheng K, Bantog C, Bayer R (2011) The impact of glycosylation on monoclonal antibody conformation and stability. MAbs 3:568–576. https://doi.org/10.4161/mabs.3.6.17922
113. Kipriyanov SM, Moldenhauer G, Little M (1997) High level production of soluble single chain antibodies in small-scale Escherichia coli cultures. Journal of Immunological Methods 200:69–77.

https://doi.org/10.1016/S0022-1759(96)00188-3

114. Witte MD, Cragnolini JJ, Dougan SK, et al (2012) Preparation of unnatural N-to-N and C-to-C protein fusions. Proceedings of the National Academy of Sciences 109:11993–11998. https://doi.org/10.1073/pnas.1205427109
115. Acosta W, Ayala J, Dolan MC, Cramer CL (2015) RTB Lectin: a novel receptor-independent delivery system for lysosomal enzyme replacement therapies. Scientific Reports 5:14144. https://doi.org/10.1038/srep14144
116. Kitaguchi D, Oda T, Enomoto T, et al (2020) Lectin drug conjugate therapy for colorectal cancer. Cancer Science 111:4548–4557. https://doi.org/10.1111/cas.14687
117. Sornay C, Vaur V, Wagner A, Chaubet G (2022) An overview of chemo- and site-selectivity aspects in the chemical conjugation of proteins. Royal Society Open Science 9:. https://doi.org/10.1098/rsos.211563
118. Goldberg SD, Cardoso RMF, Lin T, et al (2016) Engineering a targeted delivery platform using Centyrins. Protein Engineering Design and Selection. https://doi.org/10.1093/protein/gzw054
119. Wijetunge SS, Wen J, Yeh C-K, Sun Y (2018) Lectin-Conjugated Liposomes as Biocompatible, Bioadhesive Drug Carriers for the Management of Oral Ulcerative Lesions. ACS Applied Bio Materials 1:1487–1495. https://doi.org/10.1021/acsabm.8b00425
120. Chin JW, Santoro SW, Martin AB, et al (2002) Addition of p-Azido-l-phenylalanine to the Genetic Code of Escherichia coli. J Am Chem Soc 124:9026–9027. https://doi.org/10.1021/ja027007w
121. Plass T, Milles S, Koehler C, et al (2011) Genetically Encoded Copper-Free Click Chemistry. Angewandte Chemie International Edition 50:3878–3881. https://doi.org/10.1002/anie.201008178
122. Plass T, Milles S, Koehler C, et al (2012) Amino Acids for Diels-Alder Reactions in Living Cells. Angewandte Chemie International Edition 51:4166–4170. https://doi.org/10.1002/anie.201108231
123. Seitchik JL, Peeler JC, Taylor MT, et al (2012) Genetically Encoded Tetrazine Amino Acid Directs Rapid Site-Specific *in Vivo* Bioorthogonal Ligation with *trans* -Cyclooctenes. J Am Chem Soc 134:2898–2901. https://doi.org/10.1021/ja2109745
124. Greco M, Spinelli CC, de Riccardis L, et al (2021) Copper Dependent Modulation of α-Synuclein Phosphorylation in Differentiated SHSY5Y Neuroblastoma Cells. International Journal of Molecular Sciences 22:2038. https://doi.org/10.3390/ijms22042038
125. Link AJ, Tirrell DA (2003) Cell Surface Labeling of *Escherichia c oli* via Copper(I)-Catalyzed [3+2] Cycloaddition. J Am Chem Soc 125:11164–11165. https://doi.org/10.1021/ja036765z
126. Maggi A, Ruivo E, Fissers J, et al (2016) Development of a novel antibody–tetrazine conjugate for bioorthogonal pretargeting. Organic & Biomolecular Chemistry 14:7544–7551. https://doi.org/10.1039/C6OB01411A
127. Li Q, Li W, Xu K, et al (2021) PEG Linker Improves Antitumor Efficacy and Safety of Affibody-Based Drug Conjugates. International Journal of Molecular Sciences 22:1540. https://doi.org/10.3390/ijms22041540

128. Rahim MK, Kota R, Haun JB (2015) Enhancing Reactivity for Bioorthogonal Pretargeting by Unmasking Antibody-Conjugated *trans* -Cyclooctenes. Bioconjugate Chemistry 26:352–360. https://doi.org/10.1021/bc500605g
129. Rondon A, Ty N, Bequignat J-B, et al (2017) Antibody PEGylation in bioorthogonal pretargeting with trans-cyclooctene/tetrazine cycloaddition: in vitro and in vivo evaluation in colorectal cancer models. Scientific Reports 7:14918. https://doi.org/10.1038/s41598-017-15051-y
130. Brischwein K, Parr L, Pflanz S, et al (2007) Strictly Target Cell-dependent Activation of T Cells by Bispecific Single-chain Antibody Constructs of the BiTE Class. Journal of Immunotherapy 30:798–807. https://doi.org/10.1097/CJI.0b013e318156750c
131. KONTERMANN RE (2005) Recombinant bispecific antibodies for cancer therapy. Acta Pharmacologica Sinica 26:1–9. https://doi.org/10.1111/j.1745-7254.2005.00008.x
132. Peipp M, Valerius T (2002) Bispecific antibodies targeting cancer cells. Biochemical Society Transactions 30:507–511. https://doi.org/10.1042/bst0300507
133. Müller D, Karle A, Meißburger B, et al (2007) Improved Pharmacokinetics of Recombinant Bispecific Antibody Molecules by Fusion to Human Serum Albumin. Journal of Biological Chemistry 282:12650–12660. https://doi.org/10.1074/jbc.M700820200
134. Huhalov A, Chester KA (2004) Engineered single chain antibody fragments for radioimmunotherapy. The quarterly journal of nuclear medicine and molecular imaging : official publication of the Italian Association of Nuclear Medicine (AIMN) [and] the International Association of Radiopharmacology (IAR), [and] Section of the Society of. 48:279–88
135. Kipriyanov SM, Moldenhauer G, Schuhmacher J, et al (1999) Bispecific tandem diabody for tumor therapy with improved antigen binding and pharmacokinetics. Journal of Molecular Biology 293:41–56. https://doi.org/10.1006/jmbi.1999.3156
136. Klinger M, Brandl C, Zugmaier G, et al (2012) Immunopharmacologic response of patients with B-lineage acute lymphoblastic leukemia to continuous infusion of T cell–engaging CD19/CD3-bispecific BiTE antibody blinatumomab. Blood 119:6226–6233. https://doi.org/10.1182/blood-2012-01-400515
137. Kontermann Roland E. (2011) Bispecific Antibodies. Springer Berlin Heidelberg, Berlin, Heidelberg
138. Kellner C, Bruenke J, Stieglmaier J, et al (2008) A Novel CD19-directed Recombinant Bispecific Antibody Derivative With Enhanced Immune Effector Functions for Human Leukemic Cells. Journal of Immunotherapy 31:871–884. https://doi.org/10.1097/CJI.0b013e318186c8b4
139. Schubert I, Kellner C, Stein C, et al (2011) A single-chain triplebody with specificity for CD19 and CD33 mediates effective lysis of mixed lineage leukemia cells by dual targeting. MAbs 3:21–30. https://doi.org/10.4161/mabs.3.1.14057
140. Singer H, Kellner C, Lanig H, et al (2010) Effective Elimination of Acute Myeloid Leukemic Cells by Recombinant Bispecific Antibody Derivatives Directed Against CD33 and CD16. Journal of Immunotherapy 33:599–608. https://doi.org/10.1097/CJI.0b013e3181dda225

141. Chapman AP (2002) PEGylated antibodies and antibody fragments for improved therapy: a review. Advanced Drug Delivery Reviews 54:531–545. https://doi.org/10.1016/S0169-409X(02)00026-1
142. Völkel T, Korn T, Bach M, et al (2001) Optimized linker sequences for the expression of monomeric and dimeric bispecific single-chain diabodies. Protein Engineering, Design and Selection 14:815–823. https://doi.org/10.1093/protein/14.10.815
143. Smith BJ, Popplewell A, Athwal D, et al (2001) Prolonged in Vivo Residence Times of Antibody Fragments Associated with Albumin. Bioconjugate Chemistry 12:750–756. https://doi.org/10.1021/bc010003g
144. Dennis MS, Zhang M, Meng YG, et al (2002) Albumin Binding as a General Strategy for Improving the Pharmacokinetics of Proteins. Journal of Biological Chemistry 277:35035–35043. https://doi.org/10.1074/jbc.M205854200
145. Dreier T, Lorenczewski G, Brandl C, et al (2002) Extremely potent, rapid and costimulation-independent cytotoxic T-cell response against lymphoma cells catalyzed by a single-chain bispecific antibody. International Journal of Cancer 100:690–697. https://doi.org/10.1002/ijc.10557
146. Guan J, Zhang Z, Hu X, et al (2017) Cholera Toxin Subunit B Enabled Multifunctional Glioma-Targeted Drug Delivery. Advanced Healthcare Materials 6:1700709. https://doi.org/10.1002/adhm.201700709
147. Fort P, Sakai K, Luppi P-H, et al (1989) Monoaminergic, peptidergic, and cholinergic afferents to the cat facial nucleus as evidenced by a double immunostaining method with unconjugated cholera toxin as a retrograde tracer. The Journal of Comparative Neurology 283:. https://doi.org/10.1002/cne.902830209
148. Lima D, Coimbra A (1989) Morphological types of spinomesencephalic neurons in the marginal zone (Lamina I) of the rat spinal cord, as shown after retrograde labelling with cholera toxin subunit B. The Journal of Comparative Neurology 279:. https://doi.org/10.1002/cne.902790212
149. Luppi P-H, Fort P, Jouvet M (1990) Iontophoretic application of unconjugated cholera toxin B subunit (CTb) combined with immunohistochemistry of neurochemical substances: a method for transmitter identification of retrogradely labeled neurons. Brain Research 534:. https://doi.org/10.1016/0006-8993(90)90131-T
150. Luppi P-H, Sakai K, Salvert D, et al (1987) Peptidergic hypothalamic afferents to the cat nucleus raphe pallidus as revealed by a double immunostaining technique using unconjugated cholera toxin as a retrograde tracer. Brain Research 402:. https://doi.org/10.1016/0006-8993(87)90041-2
151. Siukstaite L, Rosato F, Mitrovic A, et al (2021) The Two Sweet Sides of Janus Lectin Drive Crosslinking of Liposomes to Cancer Cells and Material Uptake. Toxins (Basel) 13:792. https://doi.org/10.3390/toxins13110792
152. Ribeiro JP, Villringer S, Goyard D, et al (2018) Tailor-made Janus lectin with dual avidity assembles glycoconjugate multilayers and crosslinks protocells. Chemical Science 9:. https://doi.org/10.1039/C8SC02730G

153. Ana Valeria Meléndez, Rubí M-H Velasco Cárdenas, Simon Lagies, et al (2022) Novel lectin-based chimeric antigen receptors target Gb3-positive tumour cells. ResearchSquare. https://doi.org/10.21203/rs.3.rs-1327761/v1
154. Barbari C, Fontaine T, Parajuli P, et al (2020) Immunotherapies and Combination Strategies for Immuno-Oncology. International Journal of Molecular Sciences 21:5009. https://doi.org/10.3390/ijms21145009
155. Pellizzari A, Pang H, Lingwood CA (1992) Binding of verocytotoxin 1 to its receptor is influenced by differences in receptor fatty acid content. Biochemistry 31:1363–1370. https://doi.org/10.1021/bi00120a011
156. Schubert T, Sych T, Madl J, et al (2020) Differential recognition of lipid domains by two Gb3-binding lectins. Scientific Reports 10:9752. https://doi.org/10.1038/s41598-020-66522-8
157. Kiarash A, Boyd B, Lingwood CA (1994) Glycosphingolipid receptor function is modified by fatty acid content. Verotoxin 1 and verotoxin 2c preferentially recognize different globotriaosyl ceramide fatty acid homologues. Journal of Biological Chemistry 269:11138–11146. https://doi.org/10.1016/S0021-9258(19)78102-2
158. Binnington B, Lingwood D, Nutikka A, Lingwood CA (2002) Effect of globotriaosyl ceramide fatty acid α- hydroxylation on the binding by verotoxin 1 and verotoxin 2. Neurochemical Research 27:807–813. https://doi.org/10.1023/A:1020261125008
159. Falguières T, Mallard F, Baron C, et al (2001) Targeting of Shiga Toxin B-Subunit to Retrograde Transport Route in Association with Detergent-resistant Membranes. Molecular Biology of the Cell 12:2453–2468. https://doi.org/10.1091/mbc.12.8.2453
160. Rusconi F (2009) massXpert 2: a cross-platform software environment for polymer chemistry modelling and simulation/analysis of mass spectrometric data. Bioinformatics 25:2741–2742. https://doi.org/10.1093/bioinformatics/btp504

Figures

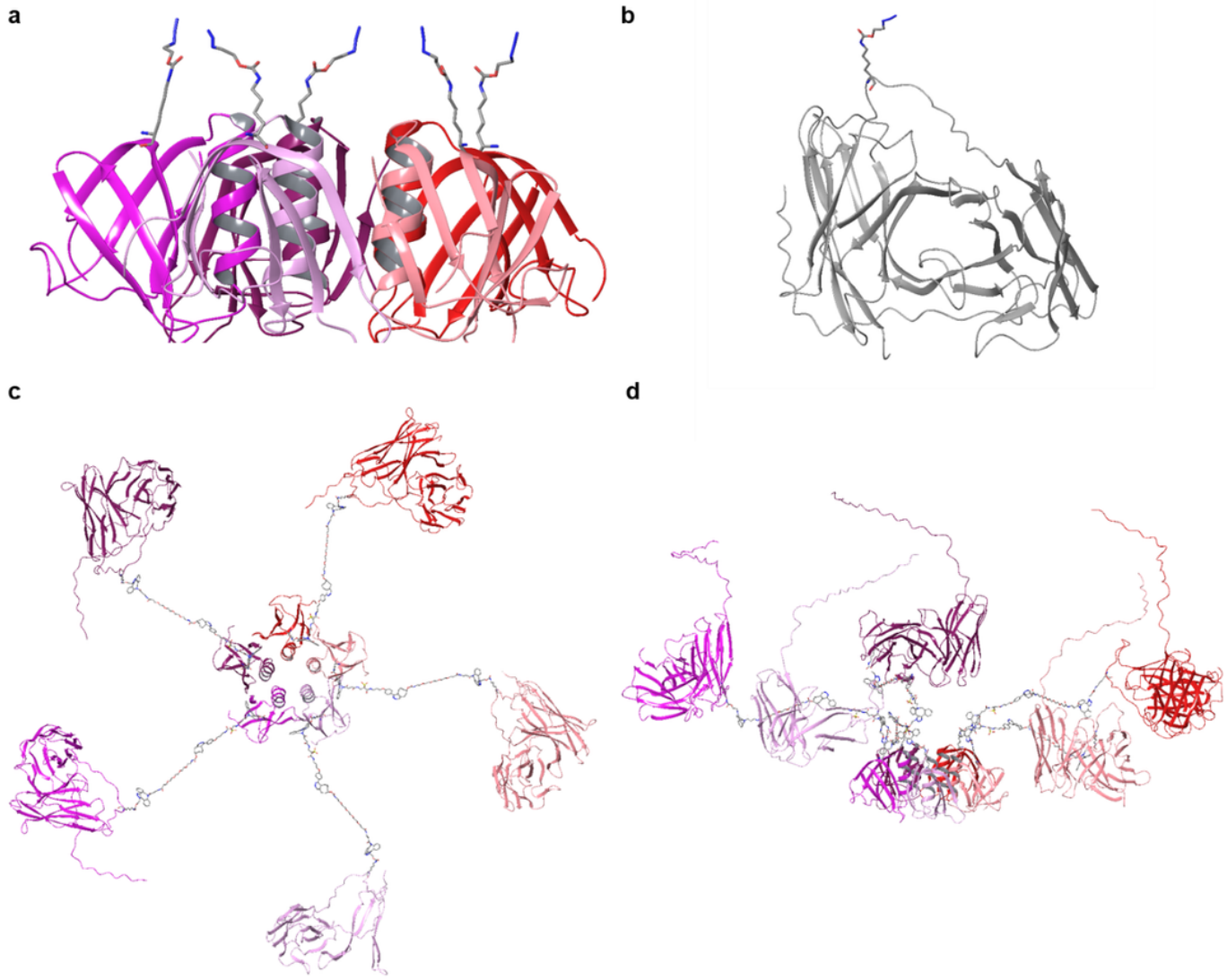

Figure 1

Atomistic models for Stx1B K9AzK, OKT3 E129AzK and Stx1B-scFv OKT3 lectibody. **a** Sideview of Stx1B containing AzK at the 9th position in each monomer. The structure is constructed based on PDB:1BOS. The five subunits of Stx1B are shown as red, pink, plum, purple and maroon ribbon cartoons; the AzK are given as sticks with grey color for C atoms, red for O atoms and blue for N atoms, H atoms are not shown for clarity. **b** Structural model of OKT3 E129AzK scFv (AzK is shown in sticks) built using homology modeling based on the template with OKT3 Fab from *Mus musculus* (PDB: 1SY6), the C-terminal fragment with low identity to the templame sequence, including 6His-tag appears as an unstructured tail. **c** Top view and **d** Side view of the Stx1B-scFv OKT3 lectibody model. Each Stx1B monomer is linked to one scFv OKT3 via DBCO-methyltetrazine-DBCO linker connected to the AzK residues. The resulting five subunits of the lectibody are shown in different colors

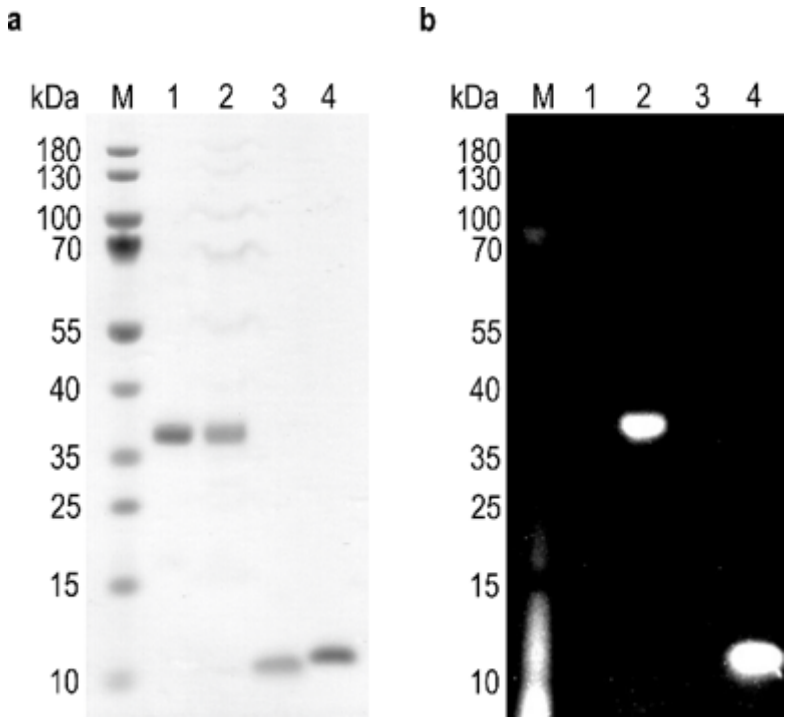

Figure 2

Confirmation of AzK incorporation in Stx1B K9AzK and scFv OKT3 E129AzK by fluorophore labelling. The purified proteins scFv OKT3 (lane 1, MWcalc30 kDa), scFv OKT3 E129AzK (lane 2, MWcalc30 kDa), Stx1B (lane 3, MWcalc 9 kDa) and Stx1B K9AzK (lane 4, MWcalc 9 kDa) were incubated with DBCO-Cy3 as detailed in the materials and methods section and then analyzed on a 4-12% SDS gel. **a** Proteins stained with Coomassie protein stain. **b** SDS gel irradiated at 635 nm before staining with Coomassie protein stain. The sizes of the molecular weight marker (M) bands are indicated on the left margin of the gels

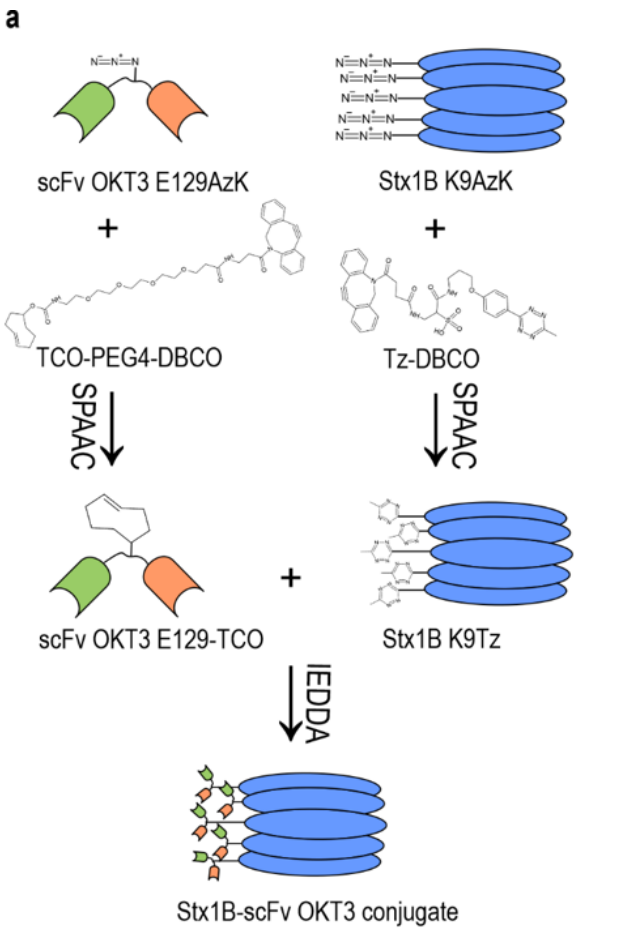

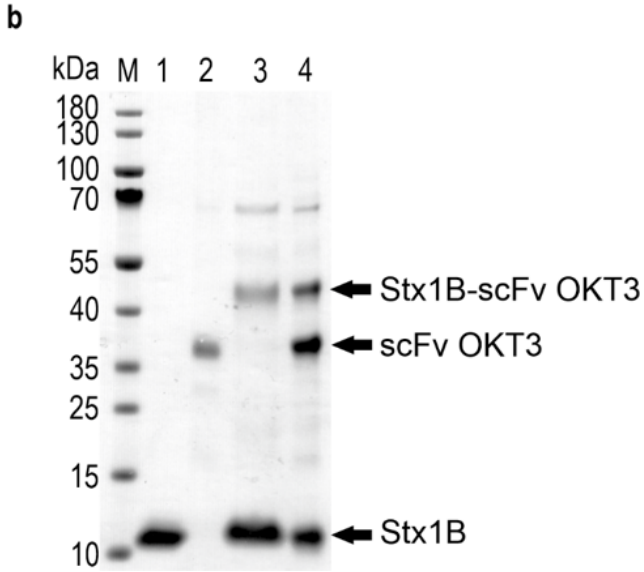

Figure 3

Formation of the Stx1B-scFv OKT3 conjugate. **a** Schematic representation of the conjugation approach. AzK was site-specifically incorporated at position E129 in scFv OKT3 and at K9 in Stx1B. Then, the azido groups in purified Stx1B K9AzK and scFv OKT3 E129AzK selectively reacted with the DBCO group on the methyltetrazine-DBCO and *trans*-cyclooctene-PEG4-DBCO linkers by SPAAC. When mixed, the methyltetrazine functionalized Stx1B K9Tz and *trans*-cyclooctene functionalized scFv OKT3 E129TCO

coupled with each other *via* an IEDDA reaction to form the Stx1B-scFv OKT3 conjugate. **b** Qualitative SDS-PAGE analysis of the IEDDA reaction mixture (lane 4). Lane 1, Stx1B K9AzK; lane 2, scFv OKT3E129AzK; lane 3, SEC purified Stx1B-scFv OKT3 conjugate. Calculated molecular weights of the individual proteins are indicated in the legend to Fig. 1. M, molecular weight marker, the band sizes are indicated on the left margin of the gel. The gel was stained with Coomassie protein stain

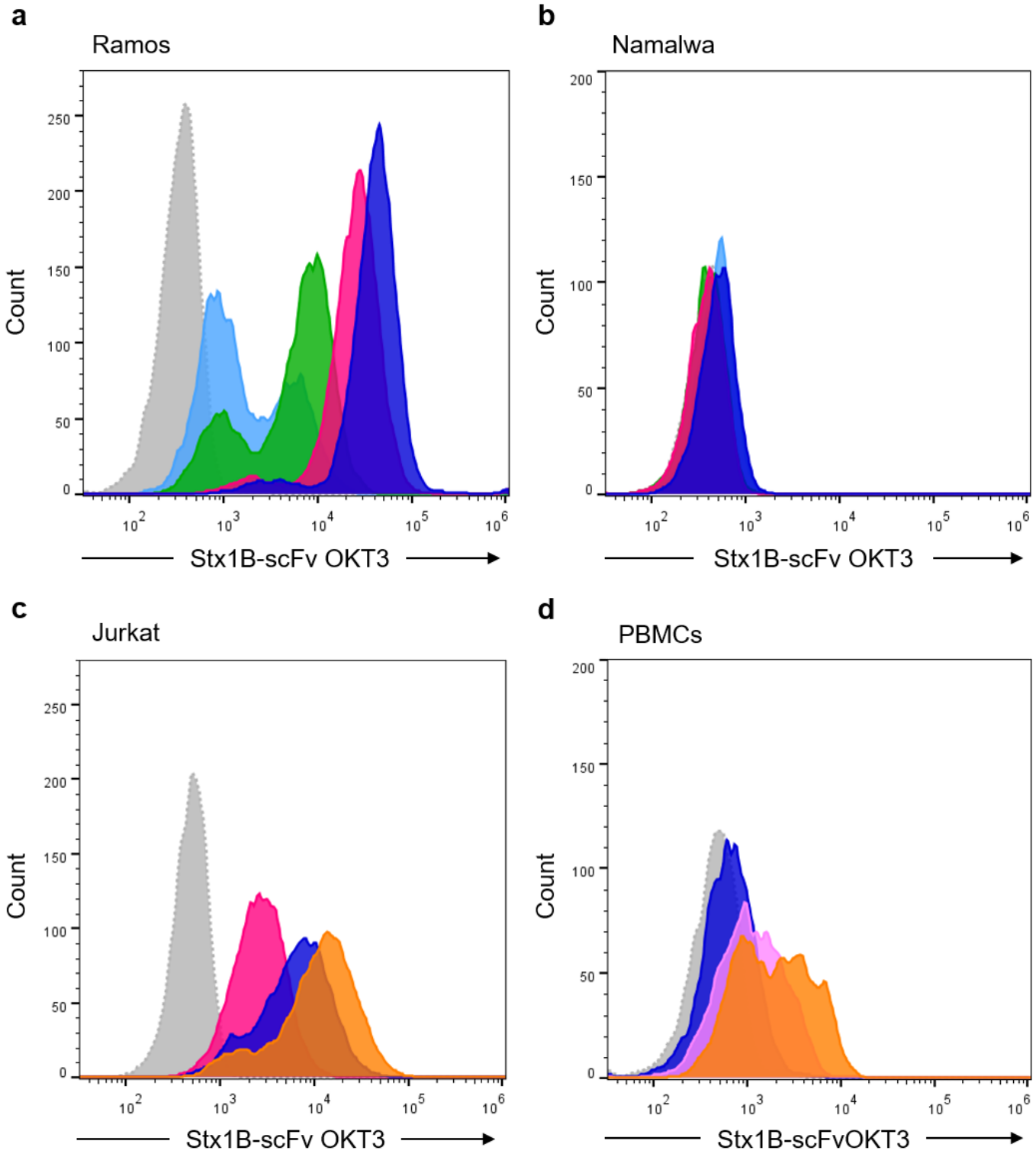

Figure 4

Dose-dependent binding of the Stx1B-scFv OKT3 lectibody to effector and target cells. Representative histograms of flow cytometry analysis of gated living **a** Ramos, **b** Namalwa, **c** Jurkat cells and **d**PBMCs from healthy donors incubated with increasing concentrations of lectibody for 30 minutes on ice. The number of cells within the live population (y-axis) is plotted against the fluorescence intensity of Stx1B-scFv OKT3 (x-axis). **a** Histograms of fluorescence intensity of Gb3+ Ramos B cells incubated with Stx1B-scFv OKT3 (dotted, grey: negative control; light blue: 0.35 nM; green: 0.7 nM; magenta: 3.5 nM; blue: 7 nM). Histograms show a dose-dependent trend in protein binding to Gb3 exposed on the surface of Ramos cells. **b** Histograms of fluorescence intensity of Namalwa B cells incubated with Stx1B-scFv OKT3 (dotted, grey: negative control; light blue: 0.35 nM; green: 0.7 nM; magenta: 3.5 nM; blue: 7 nM). Fluorescence intensity does not change following incubation of the lectibody with Gb3 cells,which excludes unspecific binding of the protein to the cell surface. **c** Histograms of fluorescence intensity of human Jurkat T cells incubated with Stx1B-scFv OKT3 (dotted, grey: negative control; magenta: 3.5 nM; blue: 7 nM; orange: 35.6 nM). **d** Histograms of fluorescence intensity of PBMCs incubated with Stx1B-scFv OKT3 (dotted, grey: negative control; blue: 7 nM; pink: 17.8 nM; orange: 35.6 nM). Binding to CD3 receptors in **c** and **d** is proven by dose-dependent shift in fluorescence intensity for the tested samples. All treated cells were stained with fluorescent anti-6-His epitope tag AF647 antibody to detect the presence of lectibody at the plasma membrane

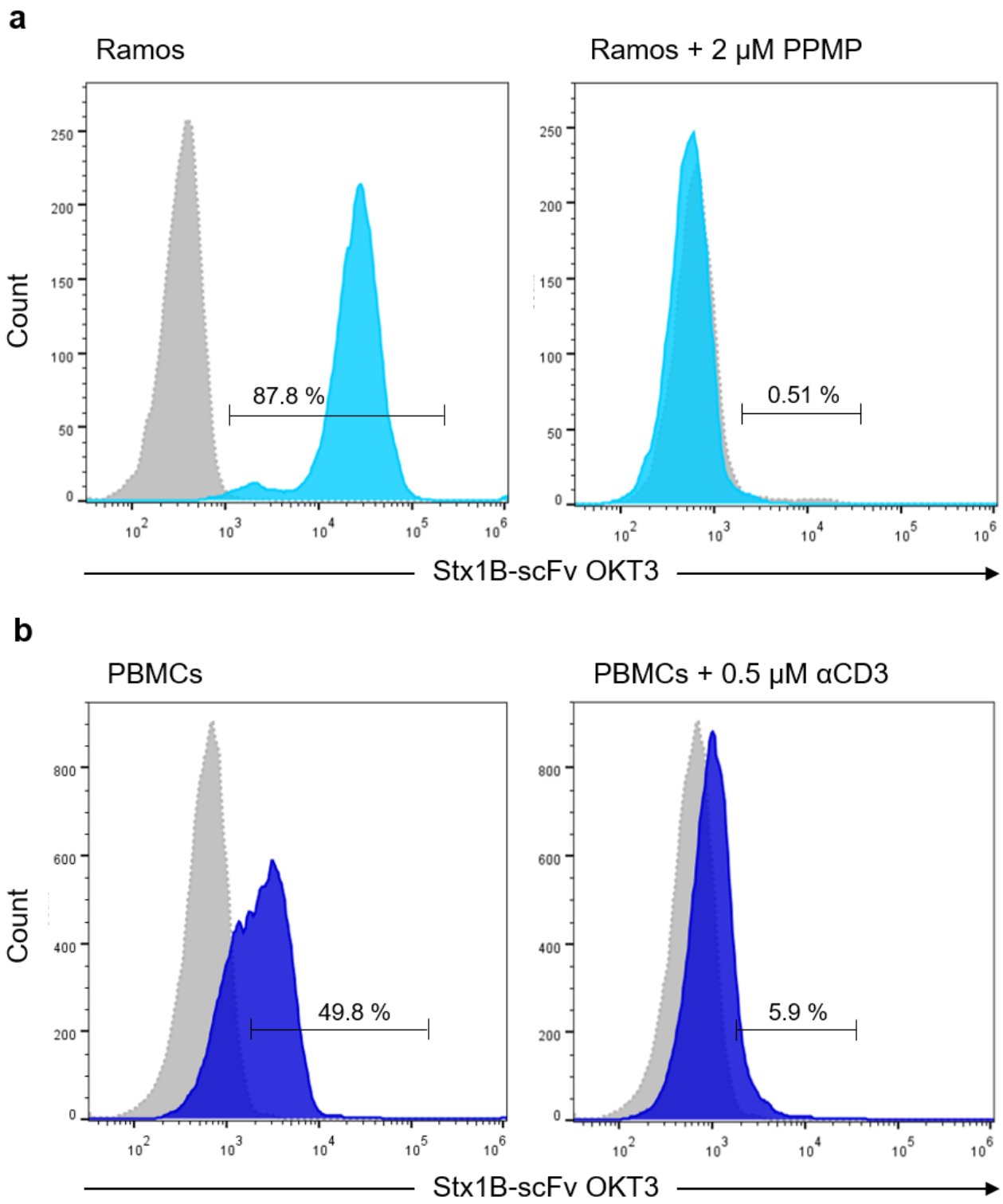

Figure 5

Binding of the Stx1B-scFv OKT3 lectibody to tumor and effector cells after depletion or saturation of receptors at the plasma membrane. Representative histograms of flow cytometry analysis of gated living **a** Ramos cells, and **b**PBMCs from healthy donors incubated with Stx1B-scFv OKT3 for 30 minutes on ice before (left panel) or after (right panel) depletion of receptors from cell surface. The number of cells within the live population (y-axis) is plotted against the fluorescence intensity of Stx1B-scFv OKT3 (x-

axis). **a** Histograms of fluorescence intensity of Gb3+ Ramos cells (left plot, untreated) incubated with Stx1B-scFv OKT3 (dotted, grey: negative control; light blue: 3.5 nM). Histograms show protein binding to Gb3 exposed on the surface. On the right plot, flow cytometry analysis of Ramos cells pre-treated for 72 hours with the GSL synthesis inhibitor PPMP and incubated with Stx1B-scFv OKT3 (dotted, grey: negative control, light blue: 3.5 nM). In the absence of Gb3, the binding of the lectibody to the plasma membrane is drastically reduced, as indicated by the shift in fluorescence intensity towards lower values. **b** Histograms of fluorescence intensity of PBMCs (left plot, untreated) incubated with Stx1B-scFv OKT3 (dotted, grey: negative control; blue: 35.6 nM). Histograms display lectibody binding to CD3 receptors present at the surface. The right plot shows flow cytometry analysis of PBMCs pre-treated with 0.5 μM of anti-human CD3 antibody for 20 minutes at room temperature, followed by incubation with Stx1B-scFv OKT3 (dotted, grey: negative control; blue: 35.6 nM). When CD3 receptors are occupied, binding of the Stx1B-scFv OKT3 lectibody to effector cells decreases remarkably

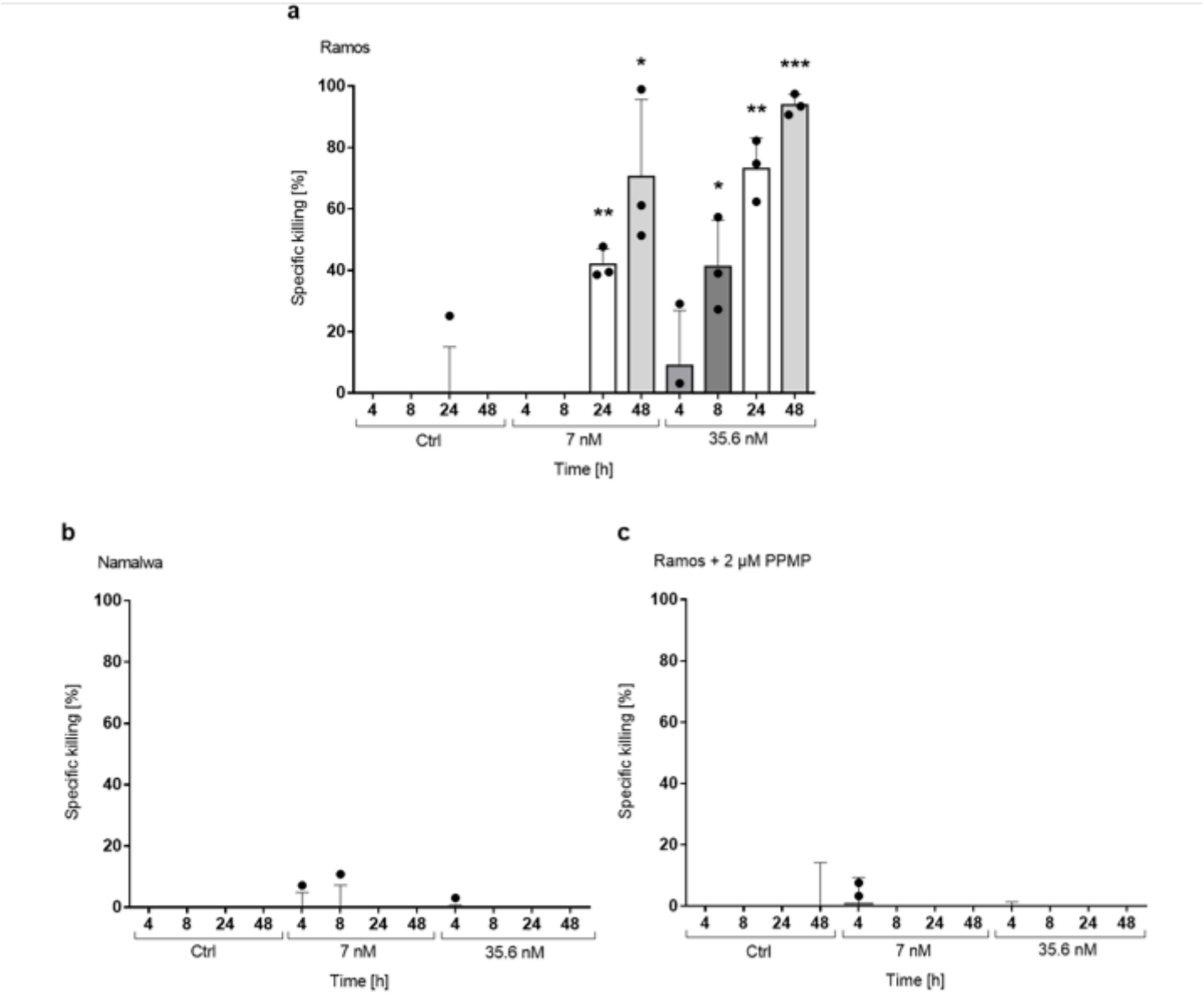

Figure 6

Induction of T cell-mediated cytotoxicity by Stx1B-scFv OKT3. Quantification of specific killing activity upon incubation of effector and target cells in presence of 7 nM or 35.6 nM lectibody. **a** Gb3+ Ramos or **b** Gb3 Namalwa cells were co-cultured in 96-well plates with PBMCs in the effector-to-target (E:T) ratio of 5:1 and purified Stx1B-scFv OKT3 lectibody. After 48 hours, about 93 % of Gb3-expressing tumor cells were eliminated in presence of 35.6 nM, while Gb3 cells did not show cytotoxicity. **c** T-cell specific killing was not detected when Ramos cells were pre-treated for 72 hours with the GSL synthesis inhibitor PPMP. Upon depletion of Gb3 from the cell surface, the lectibody did not induce redirected lysis of tumor cells. Percent viability was calculated relative to the luminescence from an equal number of input control cells and used to calculate percent specific lysis. Results are expressed as a mean ± SD (n = 3) from 3 separate experiments. Data of cell proliferation are not shown in the graph. The experiments were performed with PBMCs derived from at least 3 different donors. Statistical differences in independent, identical samples were determined with a two-tailed, unpaired t-test for control and treatment groups, at each time point. Tests with a p-value ≤ 0.05 are considered statistically significant and marked with an asterisk (*). p-values ≤ 0.01 are shown as two asterisks (**), and ≤ 0.001 are summarized with three asterisks (***)

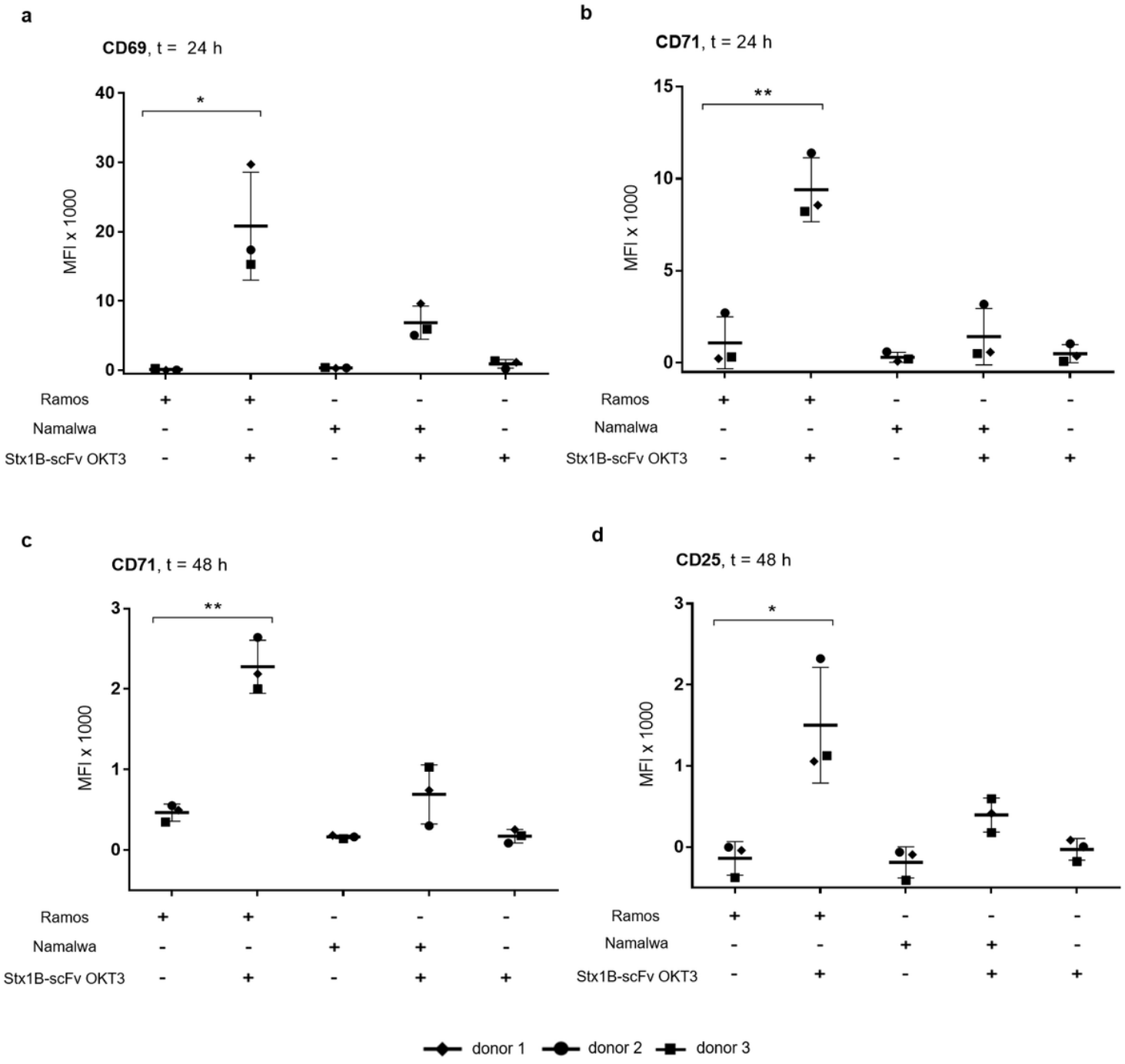

Figure 7

Up-regulation of CD8+ T cells surface markers CD69 (early), CD71 (middle) and CD25 (late) by Stx1B-scFv OKT3 lectibody. Gb3+Ramos or Gb3 Namalwa cells were co-cultured in 96-well plates with PBMCs in the effector-to-target (E:T) ratio of 5:1 and purified Stx1B-scFv OKT3 lectibody (35.6 nM). Mean Fluorescence Intensity (MFI) data from three independent donors were analyzed in flow cytometry from live CD8+ gated PBMCs. Results are expressed as a mean ± SD (*n* = 3) from two separate experiments.After 24 hours, the surface expression of T cell activation surface markers **a** CD69 and **b** CD71 was determined. **c**CD71 and **d** CD25 surface expression was monitored at 48 hours following co-incubation of target and effector cells in presence of lectibody. CD8+ T cells were significantly activated

when co-incubated with Gb3-expressing tumor cells and Stx1B-scFv OKT3, while they remained in a resting state when treated with Gb3-negative cells and lectibody. Statistical differences were determined with a two-tailed, unpaired t-test between control and each treatment group. Tests with a *p*-value ≤ 0.05 are considered statistically significant and marked with an asterisk (*), and *p*-values ≤ 0.01 are shown as two asterisks (**)

Supplementary Files

This is a list of supplementary files associated with this preprint. Click to download.

- RosatoPasupuletietalSI12092022.docx